THE UNIVERSITY OF QUEENSLAND

AUSTRALIA

Disruption of *de novo* ATP biosynthesis abolishes virulence in *Cryptococcus neoformans*

Ross Daniel Blundell

Bachelor of Science with Honours Class I in the field of Microbiology

A thesis submitted for the degree of Doctor of Philosophy at

The University of Queensland in 2016

School of Chemistry and Molecular Bioscience

Abstract

With the spread of the AIDS pandemic, opportunistic fungal pathogens like *Cryptococcus neoformans* are a growing cause of morbidity and mortality among immunocompromised populations worldwide. In part owing to a common eukaryotic ancestry that results in shared physiology between fungal and human cells, these fungal infections are difficult to treat. The limited antifungal agents currently available therefore tend to target the few key differences between the two systems to avoid inadvertently harming the host. To address the current paucity of antifungal therapeutic agents, further research into fungal-specific drug targets is required. Adenylosuccinate synthetase (AdSS) is a crucial enzyme in the ATP biosynthetic pathway, catalyzing the magnesium- and GTP-dependant formation of adenylosuccinate from inosine monophosphate and aspartate.

Over the course of my project I have investigated the potential of this enzyme as an antifungal drug target. By deleting the AdSS-encoding *ADE12* gene from the C. neoformans genome, I found that loss of AdSS function results in adenine auxotrophy in *C. neoformans*, as well as complete loss of virulence in a murine infection model. In contrast, deleting the *APH1* gene, encoding the adenine salvage enzyme adenine phosphoribosyltransferase, had no deleterious effects on cell growth or virulence in the murine model. I expressed and purified Cryptococcal AdSS from *Escherichia coli* and optimised conditions to generate high-quality AdSS protein crystals. These were used to complete X-ray diffractions studies, allowing me to determine the crystal structure of the enzyme. The structure of the enzyme's unbound form was solved first, and then used to solve the structure of the enzyme ligated with IMP and GDP. These are the first examples of an AdSS crystal structure from a fungal species. Together with enzyme kinetic studies, this structural information allowed me to compare the fungal enzyme with the human ortholog. This revealed species-specific differences that are potentially exploitable *via* rational drug design. These results validate AdSS as a promising antifungal drug target and lay a foundation for future *in silico* and *in vitro* screens for novel antifungal compounds.

Declaration by author

This thesis is composed of my original work, and contains no material previously published or written by another person except where due reference has been made in the text. I have clearly stated the contribution by others to jointly-authored works that I have included in my thesis.

I have clearly stated the contribution of others to my thesis as a whole, including statistical assistance, survey design, data analysis, significant technical procedures, professional editorial advice, and any other original research work used or reported in my thesis. The content of my thesis is the result of work I have carried out since the commencement of my research higher degree candidature and does not include a substantial part of work that has been submitted to qualify for the award of any other degree or diploma in any university or other tertiary institution. I have clearly stated which parts of my thesis, if any, have been submitted to qualify for another award.

I acknowledge that an electronic copy of my thesis must be lodged with the University Library and, subject to the policy and procedures of The University of Queensland, the thesis be made available for research and study in accordance with the Copyright Act 1968 unless a period of embargo has been approved by the Dean of the Graduate School.

I acknowledge that copyright of all material contained in my thesis resides with the copyright holder(s) of that material. Where appropriate I have obtained copyright permission from the copyright holder to reproduce material in this thesis.

Publications during candidature

Peer-reviewed papers

Blundell RD, Williams SJ, Morrow CA, Ericsson DJ, Kobe B, Fraser JA. Purification, crystallization and preliminary X-ray analysis of adenylosuccinate synthetase from the fungal pathogen Cryptococcus neoformans. Acta Crystallographica Section F. 2013;69(9):1033-6.

Ross D. Blundell, Simon J. Williams, Samantha D. M. Arras, Jessica L. Chitty,Kirsten L. Blake, Daniel J. Ericsson, Nidhi Tibrewal, Jurgen Rohr, Y. Q. Andre E. Koh, Ulrike Kappler, Avril A. B. Robertson, Mark S. Butler, Matthew A. Cooper, Bostjan Kobe, and James A. Fraser*. Disruption of de Novo Adenosine Triphosphate (ATP) Biosynthesis Abolishes Virulence in Cryptococcus neoformans*, ACS Infect. Dis., 2016, 2 (9), pp 651–663.

I. Russel Lee, Liting Yang, Gaseene Sebetso, Rebecca Allen, Thi H. N. Doan, Ross Blundell, Edmund Y. L. Lui, Carl A. Morrow, James A. Fraser. *Characterization of the Complete Uric Acid Degradation Pathway in the Fungal Pathogen Cryptococcus neoformans,* PLoS One. 2013 May 7;8(5):e64292.

Publications included in this thesis

Blundell RD, Williams SJ, Morrow CA, Ericsson DJ, Kobe B, Fraser JA. Purification, crystallization and preliminary X-ray analysis of adenylosuccinate synthetase from the fungal pathogen Cryptococcus neoformans. Acta Crystallographica Section F. 2013;69(9):1033-6.

– Incorporated as Chapter 4.

Contributor	Statement of contribution
Ross Blundell (Candidate)	Designed experiments (80%) Experimental work (95%) Data analysis (70%) Wrote the paper (85%)
Simon Williams	Designed experiments (20%) Data analysis (20%) Wrote the paper (5%)
Carl Morrow	Experimental work (5%)
Daniel Ericsson	Data analysis (10%)
James Fraser	Wrote the paper (5%)
Bostjan Kobe	Wrote the paper (5%)

Contributions by others to the thesis

Samantha Arras – Assisted in creation of *ADE12* deletion strain.
Andre Koh – Created *APH1* deletion strain.
Kirsten Blake – Created *APH1* complementation strain, assisted in completion of mouse virulence assays.
Carl Morrow – Created *ADE12* expression construct
Daniel Ericson – Data analysis.
Avril Robertson – Reagent acquisition.
Simon Williams - Conception and design of project, data analysis, thesis drafting.
Ulrike Kapler - Conception and design of project, data analysis, Thesis drafting.
James Fraser – Conception and design of project, data analysis, thesis drafting.
Bostjan Kobe - Conception and design of project, data analysis, thesis drafting.

Statement of parts of the thesis submitted to qualify for the award of another degree

None

Acknowledgements

I would like to thank my supervisors, James Fraser and Bostjan Kobe, for their support and guidance over the course of my candidature. I would extend the same thanks to Simon Williams, without whose mentorship I would never have completed this project. My thanks also go to all of my lab-mates, past and present, from both the Fraser and Kobe labs.

I would like to thank my parents and sisters for their unconditional support through my project and beyond.

I would finally like to thank the University of Queensland and the Australian Postgraduate Award scheme for supporting me financially through my project.

Keywords

Fungal pathogens, molecular biology, x-ray crystallography, structural biology, enzymology

Australian and New Zealand Standard Research Classifications (ANZSRC)

ANZSRC code: 060505, Mycology,50%

ANZSRC code: 060112, Structural Biology, 50%

Fields of Research (FoR) Classification

FoR code: 0605, microbiology, 50%
FoR code: 0601, Biochemistry & cell biology, 50%

Table of Contents

List of Figures & Tables

List of Abbreviations

AdSS – Adenylosuccinate synthetase

HIV/AIDS – Human immunodeficiency virus / Acquired immunodeficiency syndrome

IMP – Inosine monophosphate

MIC – Minimum inhibitory concentration

PBS – Phosphate-buffered saline

6-PIMP – 6-phosphoryl inosine monophosphate

RMSD - root-mean-square deviation

RPMI – Roswell Park Memorial Institute (medium)

S-AMP - Adenylosuccinate

SEC-MALS – Size-exclusion chromatography, Multiangle light scattering

YNB – Yeast nitrogen base

YPD – Yeast peptone dextrose

Chapter 1: Literature review

The past 30 years have seen the rate of immunodeficiency skyrocket. The HIV/AIDS pandemic afflicts an estimated population of 34 million [(1)]. Organ transplants are now a common surgical procedure, one that requires regimens of immunosuppressive drugs to combat rejection [(2)]. Severe burn victims undergoing heavy steroid treatment [(3)], sufferers of autoimmune disorders taking immunosuppressants [(4)], patients with congenital immunodeficiencies [(5)] or type-1 diabetes mellitus [(6)], cancer patients undergoing chemotherapy [(7)] – while improvements are made on these fronts every year, the portion of our population living with reduced or diminished immunity is still very high. These populations are vulnerable to infection by opportunistic pathogens - pathogens that are easily repelled by healthy individuals, but have devastating affects in those with compromised immune systems.

Fungal infections embody this idea of opportunistic pathogenesis. The number of serious pathogenic fungal species is relatively low, compared to the myriad diseases caused by bacteria or viruses, and those that are pathogenic are often more inconvenient rather than life threatening such as athlete's foot or thrush. On the other hand, some of the worst opportunistic infections are fungal. These opportunistic pathogens share several common traits that set them apart from other species. They often live in ecological niches that ensure patient exposure occurs on a near constant basis: some are ubiquitous in the natural environment with infectious units abundant in the air or soil, while others live as part of the microbial flora of our own bodies. They also often possess phenotypes evolved and conserved in response to their environmental niche that become virulence factors when they enter a host environment.

Three such species are recognized as the most common opportunistic fungal pathogens of the immunocompromised: the commensal yeast *Candida albicans*; the environmental filamentous fungi *Aspergillus fumigatus*; and the basidomycete yeast *Cryptococcus neoformans*, one of the primary AIDS-defining infections.

C. neoformans has a ubiquitous environmental presence, and is most abundant in soil contaminated by bird droppings. On a global scale, the most recent data from the Centers for Disease Control and Prevention estimate an affected population of up to 1.5 million people each year, with the majority of cases (up to ~1 million) occurring in sub-Saharan Africa [(8)]. Infection occurs via the lungs by inhalation of spores or desiccated yeast cells [(9)].

It is able to grow at human body temperature [10], and produces a polysaccharide capsule that protects it from opsonisation and attack by macrophages [11, 12]. It also produces the pigment melanin, which in its natural habitat may protect it from UV radiation [13]. In the human body, the pigment instead protects *C. neoformans* from the toxic free radicals deployed by the immune system [14, 15]. Even when infecting healthy patients it can lie dormant in the lungs in granulomas, re-emerging to cause serious disease if its host's immunity is compromised. In the worst infections, the fungus disseminates from the lungs and into the central nervous system to cause cryptococcal meningoencaphalitis, which is invariably fatal if left untreated.

One of the biggest difficulties in treating *C. neoformans*, and fungal infection in general, lies in the similarity of their physiology to that of human cells, which is based on their common eukaryotic ancestry. Antifungal agents tend to target the few key differences between the two systems to avoid indiscriminately damaging both host and pathogen.

One of the main differences between fungal and animal cells is the presence of ergosterol in fungal cell membranes, which is structurally distinct from cholesterol in animal cells. The azole class of antifungals target the biosynthesis of this molecule, specifically the enzyme lanosterol 14 α-demethylase. This enzyme catalyses the oxidation of the 14α-methyl group of the precursor molecule lanesterol, and the disruption of this action adversely affects the integrity and permeability of the fungal cell membrane [16-18]. Fluconazole was one of the earliest and more widely used azole compounds, and the class has been refined since its introduction 1980s, with alterations to the base triazole structure conferring increased fungistatic activity to a broader range of species. However, toxicity and bioavailability problems limit many azoles to topical use, they are fungistatic rather than fungicidal, and few new compounds are undergoing active development [19]

Another drug class that targets ergosterol are the polyenes, the most widely known of which is amphotericin B. Developed in the 1950s, polyenes achieve their fungicidal effect by binding directly to ergesterol in the fungal membrane, disrupting the integrity of the membrane by forming pore-like structures that allow the contents of the fungal cell to escape [16, 20]. Polyenes preferentially bind to ergosterol, which is what grants amphotericin B its broad-spectrum fungal-specific activity [21]. However, the selectivity of this compound for ergosterol over other sterols is weak – it is still able to form pores in lipid membranes by binding to other sterols, or without binding to anything at all [22]. This results in toxicity to animal cells, with side effects including liver and renal damage [16, 23]. Despite these

shortcomings, our mainstay antifungal treatment regimen currently relies on the polyene amphotericin B, along with the azole fluconazole, and work is ongoing to develop lipid formulations of amohotercin B that reduce its harmful side effects [(24)].

Not all antifungals target molecules that are uniquely fungal; a notable exception are the sordarin class. A natural product from the fungus *Sordaria araneosa*, sordarin was first discovered in 1971 [(25)]. Interest in the compound waned in the early 70s, but was rekindled when it performed well in a screen for protein synthesis inhibitors in *C. albicans* [(26)]. Unlike other antifungals that target the cell wall or membrane, sordarins inhibit fungal protein synthesis by stabilizing the complex between elongation factor 2 and the ribosome, arresting the translocation of the ribosome along mRNA. While this target exists in humans as well, sordarins only recognise the fungal elongation factor [(27)]. With their specificity, ease of synthesis and unique mode of action, Sordarins make for a very promising prospect for future antifungal drugs. Unfortunately, few have entered clinical development and many have had their studies discontinued [(19, 26)].

The discovery and development of new fungal-specific compounds is a high priority, and the selectivity exhibited by the sordarin drug class suggests that more fungal-specific drug targets exist outside of the traditional gross differences. One approach to repopulating the antifungal pipeline may be to apply drug design techniques towards targeting fungal-specific aspects of otherwise conserved metabolic enzymes.

The purine metabolic pathway (Fig 1) is the archetypal system in which Gertrude Elion pioneered the concept of rational drug design [(28)] which involves the use of metabolic, genetic and structural studies to identify potential targets, followed by the directed search for compounds that specifically inhibit the process in question. In this way, purine biosynthesis has served as a source of targets for therapeutic compounds for over half a century, and several drugs used today target this system; for example, the immunosuppressive agent mycophenolic acid [(29)] and the anticancer compound 6-mercaptopurine [(30)].

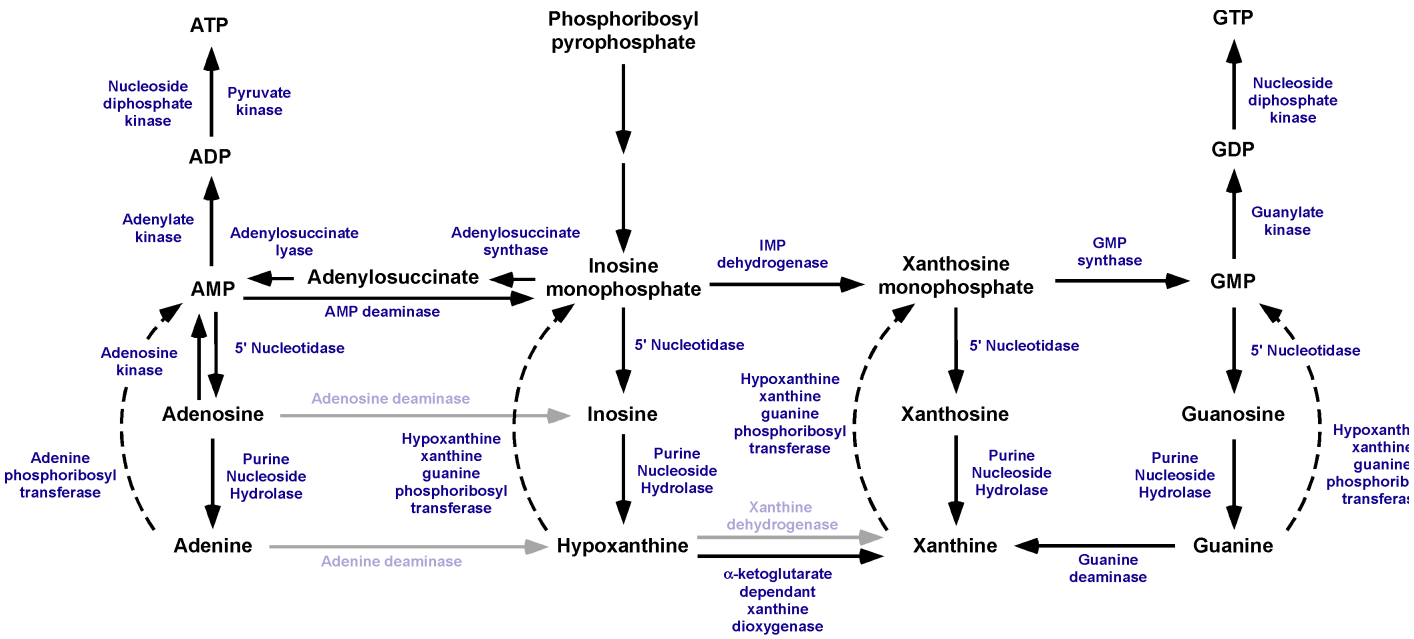

***Fig 1**: Canonical* de novo *purine biosynthetic pathway* [31]*. Reaction products are indicated in black, while responsible enzymes are indicated in blue. Greyed-out reaction steps are present in other organisms, but absent in C. neoformans.*

Purine metabolism is of particular importance in *C. neoformans* because of the disparity between the pathogen's natural niche and the human body. In nature, *C. neoformans* is most abundant in bird guano, which is extremely purine-rich. In comparison, the human body, especially the central nervous system, is purine-poor [32]. During infection, *C. neoformans* must therefore synthesise the purine nucleotides it requires *de novo*, rendering the fungus vulnerable to inhibition of its purine biosynthetic systems [31]. Previous studies by our group have begun to probe this vulnerability by characterising *C. neoformans* GTP biosynthetic enzyme IMP dehydrogenase [31, 33]. These studies laid a foundation for the search for new inhibitors of this enzyme and illuminated the potential of *de novo* purine biosynthesis as a source of antifungal targets. Here we have evaluated the other branch of the purine biosynthesis pathway, ATP biosynthesis. Adenylosuccinate synthetase (AdSS) catalyzes the first committed step in the biosynthesis of ATP, the formation of adenylosuccinate (s-AMP) from inosine monophosphate (IMP) and aspartate. AdSS is an essential enzyme for most organisms and cell types studied thus far, with the exception of mature human erythrocytes [34] and certain obligate parasites [35].

While bacteria and most eukaryotes have only one form of AdSS, in vertebrates the enzyme exists as both a basic/muscle form and an acidic/non-muscle form, each encoded by different genes. These isoforms are believed to play slightly differing roles in purine

metabolism – the acidic form is involved in *de novo* purine biosynthesis, while the basic form helps regulate ATP/GTP homeostasis [(36-38)].

The AdSS mediated production of s-AMP is GTP- and Mg^{2+}-dependent and proceeds *via* two steps. First, the γ-phosphate from GTP is transferred to the 6-oxygen of IMP, forming the intermediate 6-phosphoryl IMP (6-PIMP). The 6-phosphoryl group is then displaced by the α-amino group of aspartate to form adenylosuccinate [(39)].

The first reported crystal structure of an AdSS enzyme was from *Escherichia coli*, and it remains the best characterised form of this enzyme (Fig 2) [(40, 41)]. *E. coli* AdSS is a functional homodimer, with its structure comprised of a nine-stranded β-sheet backbone and four large subdomains. Directed mutagenesis studies have identified a deep crevice between these domains as the enzyme's active site [(42, 43)] and it is only when the enzyme binds IMP that this active site becomes fully ordered [(44)]. Without ligands, AdSS is believed to exist in an equilibrium between dimeric and monomeric states [(45)]. IMP binding stabilises the coupling of the monomers into a functional homodimer, shifting the equilibrium in favour of the dimer [(45, 46)]. While both AdSS subunits contain a separate active site, a conserved arginine side-chain from each subunit projects across the dimeric interface and contributes to the active site of the other subunit. AdSS must therefore be in its dimeric conformation to possess a complete active site, as this arginine assists the binding of IMP and GTP [(40, 47)]. Subsequent studies showed that the structure and mechanism of *E. coli* AdSS is conserved in other species including *Plasmodium falciparum* [(48)], *Arabidopsis thaliana* [(49)] and mice [(50)]. Prior to this work, no structure of AdSS from a fungal species had been reported.

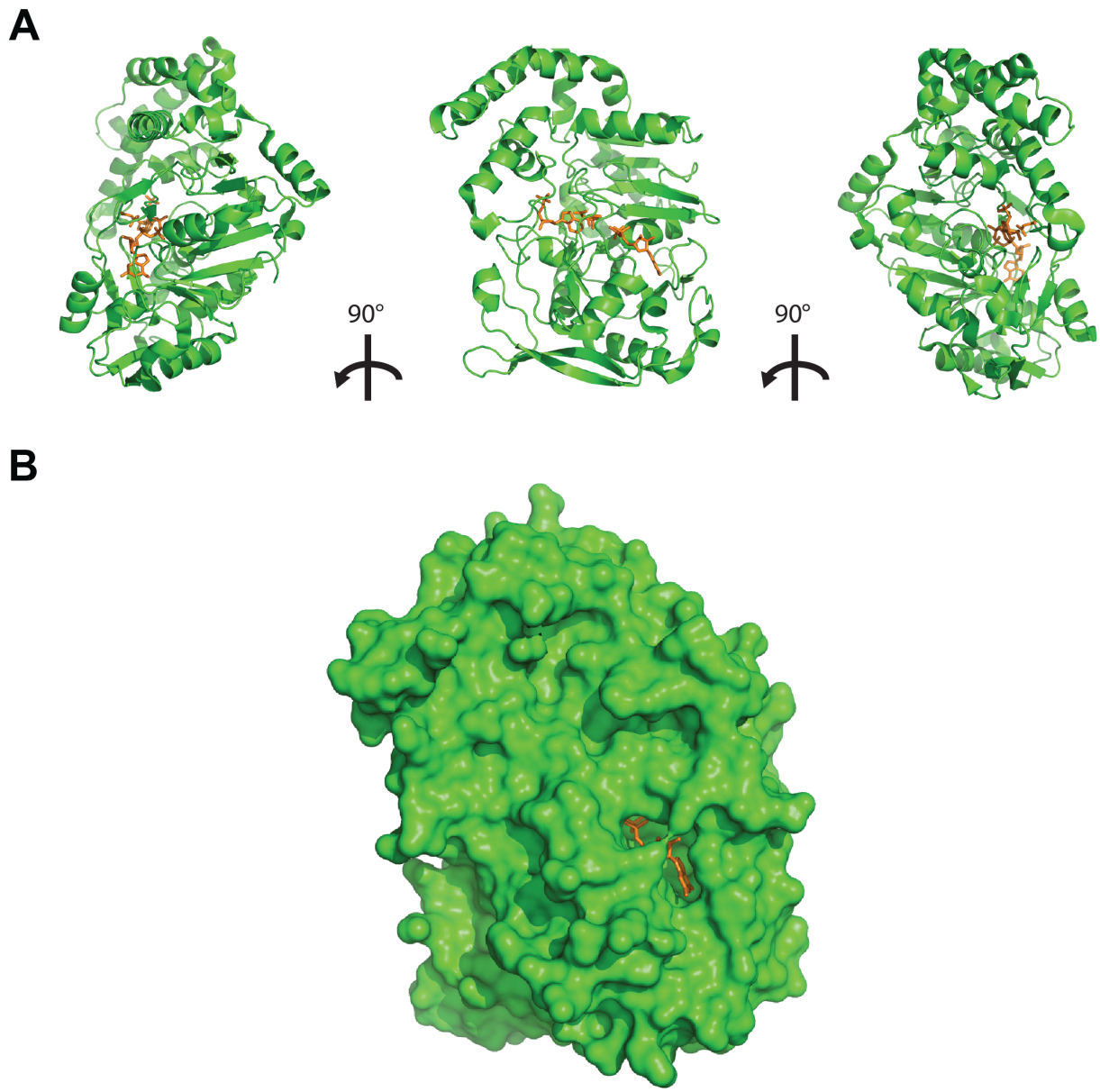

***Fig 2**: Crystal structure of AdSS from E. coli, representing the general model of AdSS structure. (A) Crystal structure of E. coli AdSS monomer (shown in cartoon form) bound to IMP and GDP and rotated clockwise in 90º increments. Bound ligands IMP and GDP are shown in stick form, colored orange. (B) Surface mesh of E. coli AdSS monomer, displaying active site face. Flexible loops are shown in closed position over the active-site cleft. IMP is visible in stick form, colored orange. The PDB ID for the E. coli structure is 2GCQ.*

There are three well-characterised inhibitors of AdSS, each of which targets a different aspect of this enzymatic reaction: alanosine, hadacidin, and hydantocidin (Fig 3). None of these inhibitors have so far been shown to have any antifungal activity.

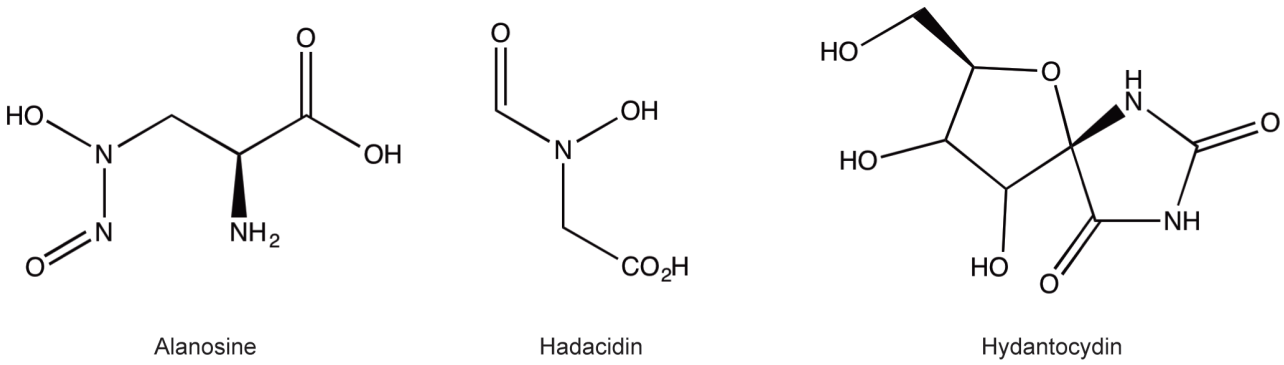

Alanosine Hadacidin Hydantocydin

Fig 3*: Structures of inhibitors of AdSS.*

Alanosine is a compound produced by *Streptomyces alanosinicus*, found to have antibiotic, antitumor, antiviral and immunosuppressive activities [(51)]. The compound inhibits AdSS's activity [(52)] but has no significant activity against AdSS on its own [(53)]. Instead, alanosine is conjugated with 5-amino-4-imidazolecarboxylic acid ribonucleotide (AICOR) by AICAR synthetase, an enzyme involved in *de novo* IMP synthesis. The resulting molecule L-ananosyl-AICOR is competitive with IMP [(54)]. Phase II clinical trials have been performed testing alanosine's effectiveness against Methylthioadenosine phosphorylase (MTAP)-deficient tumours, which are reliant on *de novo* purine biosynthesis [(55)]. Unfortunately, the drug was found to be ineffective and has not seen further clinical development.

Hadacidin is an antitumor and anti-microbial compound first isolated in 1962 from the broth of *Penicillium frequentans* [(56)]. Initially named after its ability to inhibit the growth of human adenocarcinoma cells, Hadacidin also has inhibitory activity against plants [(57)] and bacteria [(58)]. It is a catalytically inactive analogue of L-aspartate, the addition of which has been found to competitively inhibit the compound's activity [(59)]. Hadacidin appears to possess no other biological function besides the inhibition of AdSS [(60)]. Analogues of hadacdin have also been tested for activity against AdSS [(61)], but the compound has not been developed further since.

Finally, Hydantocidin is produced by *Streptomyces hygroscopicus*, and was first discovered in 1990. It is an herbicide with a broad range of activity against plants, but no toxicity against microbial or animal organisms [(62)]. The compound was found to be a pro-drug that binds to AdSS after being phosphorylated to hydantocidin 5'-monophosphate. Activated hydantocidin achieves its inhibitory effect by mimicking AMP [(63)]. Physically linking hydantocidin and hadacidin together creates a bi-substrate hybrid inhibitor with potent activity against AdSS in vitro [(64)], but the compound has not seen further development and hydantocidin does not see commercial use.

During my project, I have investigated the potential of AdSS as a candidate antifungal drug target in the fungal pathogen *C. neoformans*. I have assessed the impact of loss of AdSS function on *C. neoformans* growth, virulence factor production and virulence in an animal model, characterised the kinetic properties of the cryptococcal enzyme and determined the *C. neoformans* AdSS crystal structure. Collectively, my work validates AdSS as a promising antifungal drug target and provides a platform for future drug design studies.

Chapter 2: Materials and methods

Bioinformatic analysis

The *C. neoformans* var. *grubii* genome sequence was reported by Janbon *et al.* [65]. AdSS- and Aph1-encoding genes were identified in the *C. neoformans* genome by reciprocal best-hit BLAST analysis against the genome of *Saccharomyces cerevisiae.*

Strains and media

C. neoformans H99 is the type-strain used in C. neoformans research worldwide[65]. H99 was cultured on YPD (2% bacto-peptone, 2% agar, 1% yeast extract, 2% glucose) or YNB (Becton Dickinson, USA) supplemented with 2% glucose and 100 mM ammonium sulfate at 30 ˚C. AdSS deletion mutants are adenine auxotrophs and, as such, were grown on minimal YNB media supplemented with 2% glucose, 100 mM ammonium sulfate and 2 mM adenine for all manipulations, unless otherwise stated. Cloning and plasmid preparation was performed in *E. coli* strain Mach1 (Life Technologies, USA). Genomic DNA for *E. coli* gene isolation was prepared from strain K12. Recombinant *C. neoformans* AdSS was heterologously expressed in *E. coli* strain BL21(DE3) (Novagen, Germany). Nourseothricin (clonNAT) was purchased from Werner BioAgents (Jena Bioscience, Germany), and G418 was purchased from Sigma, USA.

Cloning and chimera construction

All primers used in the study are listed in Table S1. The *ADE12* deletion construct was created by using overlap PCR to join the following fragments: The *ADE12* 5′ region (primers UQ1742 and UQ1743, H99 genomic DNA template); the G418 resistance marker *NEO* (UQ1830 and UQ1831, plasmid pJAF1 template [66]); and the *ADE12* 3′ region (UQ1744 and UQ1745, H99 genomic DNA template). The *APH1* deletion construct was created by using overlap PCR to join the following fragments: The *APH1* 5′ region (primers UQ1750 and UQ1751, H99 genomic DNA template); the G418 resistance marker *NEO* (UQ1834 and UQ1835, plasmid pJAF1 template); and the *APH1* 3′ region (UQ1752 and UQ1753, H99 genomic DNA template). Sequencing of plasmid constructs was performed at the Australian Genome Research Facility (Brisbane, Australia) and sequence traces were analyzed using Sequencher 4.7 (Gene Codes, USA). This construct was provided by Andre Koh.

To create complementation constructs, *ADE12* from *C. neoformans* strain H99 was TOPO-cloned as a PCR fragment (primers UQ1742 and UQ1745) into pCR2.1 TOPO (Life Technologies), then subcloned as a restriction fragment (EcoRV and Apa1) into the nourseothricin acetyltransferase (NAT) vector pCH233 to give the plasmid pAK07 [(67)]. This construct was provided by Andre Koh. *APH1* from *C. neoformans* strain H99 was TOPO-cloned as a PCR fragment (primers UQ1750 and UQ1753) into pCR2.1 TOPO, then subcloned as a restriction fragment (SacI and NheI) into the nourseothricin acetyltransferase (NAT) vector pSDMA25 to give the plasmid pKLB01 [(68)]. This construct was provided by Kirsten Blake. All wild-type strains utilized and mutant strains created are listed in Table S2.

To create a construct for expression of *C. neoformans* AdSS in *E. coli*, total RNA was isolated from *C. neoformans* var. *grubii* strain H99 using TRIzol (Invitrogen). Intron-free cDNA was then synthesized using a Bioline cDNA synthesis kit (Bioline). *ADE12* was PCR-amplified, with unique restriction sites (BamHI and PstI) introduced via the specifically designed primers UQ2259 and UQ2260. The PCR product was then cloned into the TOPO pCR2.1 vector (Invitrogen), sequenced and ligated into BamHI/PstI-cut pQE-30 expression vector (Qiagen), which introduced an N-terminal 6×His tag (MRGSHHHHHHGS). This construct was provided by Dr. Carl Morrow.

Molecular techniques

Standard molecular techniques were performed as described by Sambrook *et al*. [(69)]. *C. neoformans* genomic DNA for Southern blot analysis was prepared as described [(70)]. Overlap PCR, gene deletion transformation and mutant complementation was performed as described [(71-74)] *via* particle delivery using a BioRad He-1000 Biolistic Device (Bio-Rad, USA). For Southern hybridizations, DNA was digested with the indicated enzymes, electrophoresed on 1% TAE- agarose gels and blotted onto Hybond-XL membrane (GE Healthcare, UK) using standard procedures. Probes were generated using the DECAprime 2 Random Primed DNA Labeling Kit (Thermo Fisher, US) with PCR products amplified from H99 template DNA radiolabelled with α^{32}P dCTP (PerkinElmer, USA). Blots were hybridized overnight at 65 ºC and membranes were exposed onto Fuji Super RX medical X-ray film (Fujifilm, Japan). Oligonucleotides used are detailed in Table S1.

Virulence factor assays

Melanization assays were performed at 30 ˚C and 37 ˚C on solid l-DOPA media supplemented with 10 mM asparagine [75]. Phospholipase B assays were performed on solid Sabouraud dextrose agar with 8% egg yolk at 30 ˚C and 37 ˚C [76]. Capsule growth was induced by overnight growth in RPMI 1640 media plus 2% glucose and 10% fetal bovine serum, and stained with India-ink (Becton Dickinson) to visualize the capsule. Capsule sizes were determined from phase contrast images, as described previously [31]. All media was supplemented with 5 mM adenine to enable growth of auxotrophic strains.

Minimum inhibitory concentration assays

MIC susceptibility testing for hadacidin was performed using the broth microdilution method according to CLSI (CLSI M27-A2) modified for *Cryptococcus neoformans* [77]. The fungal species panel included *C. neoformans* H99, *C. neoformans* ATCC-90113, *C. albicans* ATCC-90028, *Candida parapsilopsis* ATCC-22019, *Candida galbrata* ATCC-90030, and *Aspergillus fumigatus* MYA-3626. The fungal panel was tested in a 96-well plate format in triplicate. Approximately 170 fungal cells in liquid YNB (yeast species) supplemented with 2% glucose and 100 mM ammonium sulfate or RPMI 1640 (*A. fumigatus*) media supplemented with 100 mM ammonium sulfate were grown with either hadacidin or positive controls amphotericin B and fluconazole in a 2-fold, 12-step serial dilution across the long axis of the plate, starting at 0.1 mg/mL. Plates were inspected for cell growth at 24, 48 and 72 hours post-inoculation, and a Molecular Devices SpectraMax 250 plate-reader was used to measure the OD_{600} of each well at 72h.

Murine virulence assays and organ burden analysis

Assessment of cryptococcal virulence in the murine model system was performed as described previously [78, 79]. For each strain, ten 6-week old female BALB/c mice were infected *via* nasal inhalation with a 50 µL drop of PBS containing 5×10^5 fungal cells. Mice were weighed daily and euthanized by CO_2 inhalation once body weight had dropped below 80% of their starting weight, symptoms of infection were judged to be severe, or on the final day of the experiment. For organ burden analysis, brain, lungs, liver, spleen and kidneys were harvested from euthanized mice. Organs were weighed, homogenized and plated in serial dilution on YPD media to determine colony-forming units per gram of organ. Organ burden data was analyzed by 1-way ANOVA with Sidak's multiple comparison post-test using GraphPad Prism 6.0.

Ethics Statement

This study was carried out in strict accordance with the recommendations in the Australian Code of Practice for the Care and Use of Animals for Scientific Purposes by the National Health and Medical Research Council. The protocol was approved by the Molecular Biosciences Animal Ethics Committee (AEC) of The University of Queensland (AEC approval no. SCMB/439/13/UQ/NHMRC). Infection was performed under methoxyflurane anesthesia, and all efforts were made to minimize suffering through adherence to the Guidelines to Promote the Wellbeing of Animals Used for Scientific Purposes as put forward by the National Health and Medical Research Council (Australia).

Expression and purification of *C. neoformans* AdSS

Early failed cloning efforts strongly suggested that the *ADE12* pQE30 construct was toxic in *E. coli*. The ligation was therefore transformed into competent BL21(DE3)pLysS *E. coli* cells (Promega) expressing the pREP4 repressor plasmid to reduce “leaky” expression. Transformed cells were grown in terrific broth (TB) media with 100 µg/mL ampicillin, 35 µg/mL kanamycin and 12.5 µg/mL chloramphenicol. Cultures were incubated at 37 ˚C until they reached an OD_{600} of approximately 1.0, after which they were induced with 1 mM IPTG and grown at 20 ˚C for 5 hours. Cell pellets were harvested and resuspended in lysis buffer (50 mM HEPES pH 8, 300 mM NaCl, 1 mM DTT, 30 mM imidazole, and 1 mM PMSF) then lysed by sonication. AdSS was purified via Ni-immobilised metal-affinity chromatography using HisTrap fast flow columns (GE Healthcare) and eluted over 20 column volumes in a linear gradient of 30-500 mM imidazole. A single main elution peak was seen. Fractions corresponding to this peak were combined and further separated over a Superdex 200 size-exclusion chromatography (SEC) column (GE Healthcare) equilibrated in SEC buffer (10 mM HEPES ph7.5, 150 mM NaCl, 1 mM DTT) using an ÄKTA-Purifier FPLC system (GE Healthcare). Peak fractions were combined and concentrated to approximately 16 mg/mL at >99% purity estimated by Coomassie-stained SDS-PAGE gel and snap-frozen for storage at -80 ˚C .

Crystallization of *C. neoformans* AdSS

Purified AdSS was initially screened in its Apo form, without any additional ligands or cofactors. All crystallization experiments were performed using the hanging drop vapor diffusion method at 293 K. Initial screening for crystallization conditions was performed using the Index, Peg/Ion 1 and Peg/Ion 2 (Hampton Research), Pact Premier and JCSG

(Qiagen), Proplex and Morpheus (Molecular Dimensions), and Synergy (Jena Biosciences) commercial screening plates. Plates were set up by a Mosquito Nanodrop crystallization robot (TTP LabTech), with each drop containing 100 nL protein solution and 100 nL reservoir solution inverted over reservoirs of 100 µL. A Rock Imager system (Formulatrix) was used to monitor crystal growth in the drops. Crystals were found in approximately 200 conditions. The most promising candidates were chosen for further screening and optimization. Final diffraction-quality crystals were obtained using a condition from the PACT screen. Drops containing 1 µL of protein solution at 16 mg/mL and 1 µL of reservoir solution (0.1 M BisTris propane pH 8, 0.2 M sodium bromide, 17% polyethylene glycol 3350) were streak-seeded from non-suitable AdSS crystals after 30 minutes equilibration over 500 µL reservoirs. Long rectangular crystals of approximately 0.5 × 0.05 × 0.05 mm formed after 24-48 hours.

In addition, purified AdSS was also co-crystallized with its substrates IMP, GTP, hadacidin and magnesium. For co-crystallization, the protein was screened and crystallized as above, with the following modifications: final diffraction-quality crystals were obtained using a condition from the PEG/Ion 2 crystallization screen (Hampton research) in which no crystals were detected during screening of the apo-enzyme. Drops containing 1 µL of co-crystallization solution (AdSS protein at 16 mg/mL in gel filtration buffer from [80], 5 mM IMP, 5 mM GTP, 5 mM hadacidin, 50 mM magnesium acetate) and 1 µL of reservoir solution (0.1 M ammonium citrate tribasic, 18% PEG3350) were equilibrated over 500 µL reservoirs. Long rectangular crystals formed at 18 ˚C after 24-48 hours, with no need for streak-seeding.

X-ray diffraction data collection and processing

X-ray diffraction data from AdSS crystals was collected to a resolution of 2.2 Å for the apo-enzyme and 1.55 Å for the ligated enzyme. The data was collected on the MX2 beamline at the Australian Synchrotron, indexed and integrated using XDS [81] and scaled with AIMLESS within the CCP4 suite [82].

The structure of apo-AdSS was solved by molecular replacement using Phaser [83] with the structure of the muscle isoform of mouse AdSS (PDB ID: 1J4B, 55% amino-acid sequence identity) as a template. Automated model building was performed using Phenix.autobuild [84, 85] and refinement was performed using Phenix.refine coupled with iterative manual adjustments using Coot [86, 87]. The structure of ligated AdSS was solved by the same

method, using the apo-AdSS structure previously generated as the template for molecular replacement. Figures were generated with PyMOL (http://www.pymol.org). Data collection and refinement statistics for both structures are listed in Table S3. Atomic coordinates and structure factors of both the apo-AdSS and ligand-bound structures have been deposited in the Protein Data Bank, www.pdb.org (PDB IDs: 5I33 and 5I34 respectively).

Multiangle laser light scattering with size exclusion chromatography

Size-exclusion chromatography (SEC) – multiangle laser light scattering (MALS) was performed using a Dawn Heleos II 18-angle light-scattering detector coupled with an OptilabrEX refractive index detector (Wyatt Technology, Santa Barbara, CA, USA) and inline Superdex 200 10/300 size exclusion column (GE Healthcare). Experiments were performed at an AdSS concentration of 5 mg/mL in SEC buffer (10 mM HEPES pH 7.5, 150 mM NaCl, 1 mM DTT) at room temperature, with a flow rate of 0.5 mL/min.

Steady-state enzyme kinetics and inhibitor analysis

All enzyme assays were performed as previously described [88] with some modifications. Enzymatic assays were performed at 25 ˚C in triplicate by monitoring the production of adenylosuccinate at 280 nm (ε = 11.7 mM^{-1} cm^{-1}) for 5 min using a Varian Cary 60 spectrophotometer (Agilent Technologies, USA). Assays were performed in 10 mm optical quartz cuvettes (Starna Scientific, UK). Each assay was performed in a total volume of 1 mL standard AdSS assay buffer (50 mM potassium phosphate pH 7.2, 8 mM magnesium acetate) containing 4 µg of purified enzyme, 100 µM GTP, 150 µM IMP and 7 mM aspartate. For K_M determination, IMP, GTP and aspartate concentrations were varied over ranges of: 2.5 to 200 µM for GTP; 9.5 to 300 µM for IMP; and 100 µM to 15 mM for aspartate. Direct nonlinear fitting of the data to the Michaelis-Menten equation was performed using Prism 6 (GraphPad Software, USA).

Inhibitor IC_{50} values were determined by adding increasing concentrations of hadacidin (40 to 640 µM, dissolved in water) to the aforementioned standard AdSS assay condition and determining the reaction velocity. Non-treated cells and solvent-only controls were also included. Assays were performed at 25 ˚C in triplicate by monitoring the production of adenylosuccinate at 280 nm (ε = 11.7 mM^{-1} cm^{-1}) for 5 min using a Varian Cary 60 spectrophotometer. Nonlinear fitting of the data to a single-phase exponential decay equation was performed using GraphPad Prism 6.0.

Chapter 3: Characterization of AdSS

Identification of the AdSS-encoding gene in *C. neoformans*

In order to begin our characterization of AdSS from *C. neoformans*, we first identified its corresponding gene. As the AdSS-encoding gene from *S. cerevisiae* is well-characterized, it was used in a reciprocal best-hit BLAST analysis to identify the equivalent gene from the published *C. neoformans* genome [(65)]. Only one hit was obtained, indicating that the gene is present in a single copy located on chromosome 3. This gene has the ORF designation CNAG_02858 and was named *ADE12* after the *S. cerevisiae* ortholog, with which its predicted product is 61% identical at the amino acid level. It is 54% identical to both the acidic and basic isoforms of the human ortholog and 42% identical to the enzyme in *E. coli*. Areas of high conservation are found around predicted active site residues (Fig S1).

Loss of AdSS function results in adenine auxotrophy

To verify the function of the identified gene, we employed biolistic transformation to delete it from the genome of *C. neoformans* type strain H99. In brief, DNA constructs consisting of an antibiotic resistance marker flanked by the sequences immediately 5' and 3' of *ADE12* in the *C. neoformans* genome. These constructs were then precipitated onto gold microbeads. Transformations were performed using a biolistic device, which uses compressed air to fire the DNA-coated beads into a lawn of fungal cells grown on standard media. Gold-impregnated cells are then scraped into solution and spread onto selective media. In successfully transformed cells, homologous recombination occurs between the fungal genome and the identical 5' and 3' flanking regions of the deletion construct, replacing the gene of interest with the payload resistance cassette. This procedure was carried out by Samantha Arras.

The resulting *ade12*Δ strain was an adenine auxotroph, unable to grow on either rich or minimal media without supplemental adenine (Fig 4). Adenine prototrophy was restored when the deletion strain was transformed with the wild-type *ADE12* gene, creating the complemented derivative strain *ade12*Δ*+ADE12*. Auxotrophy was detected in the *ade12*Δ strain at both optimal growth temperature (30 ºC) and at human body temperature (37 ºC), and is consistent with previous work involving the GTP branch of the de novo purine synthesis pathway, where loss of IMP dehydrogenase activity resulted in guanine auxotrophy [(31)]. The deletion and re-introduction of the *ADE12* gene was confirmed by Southern blot analysis (data not shown).

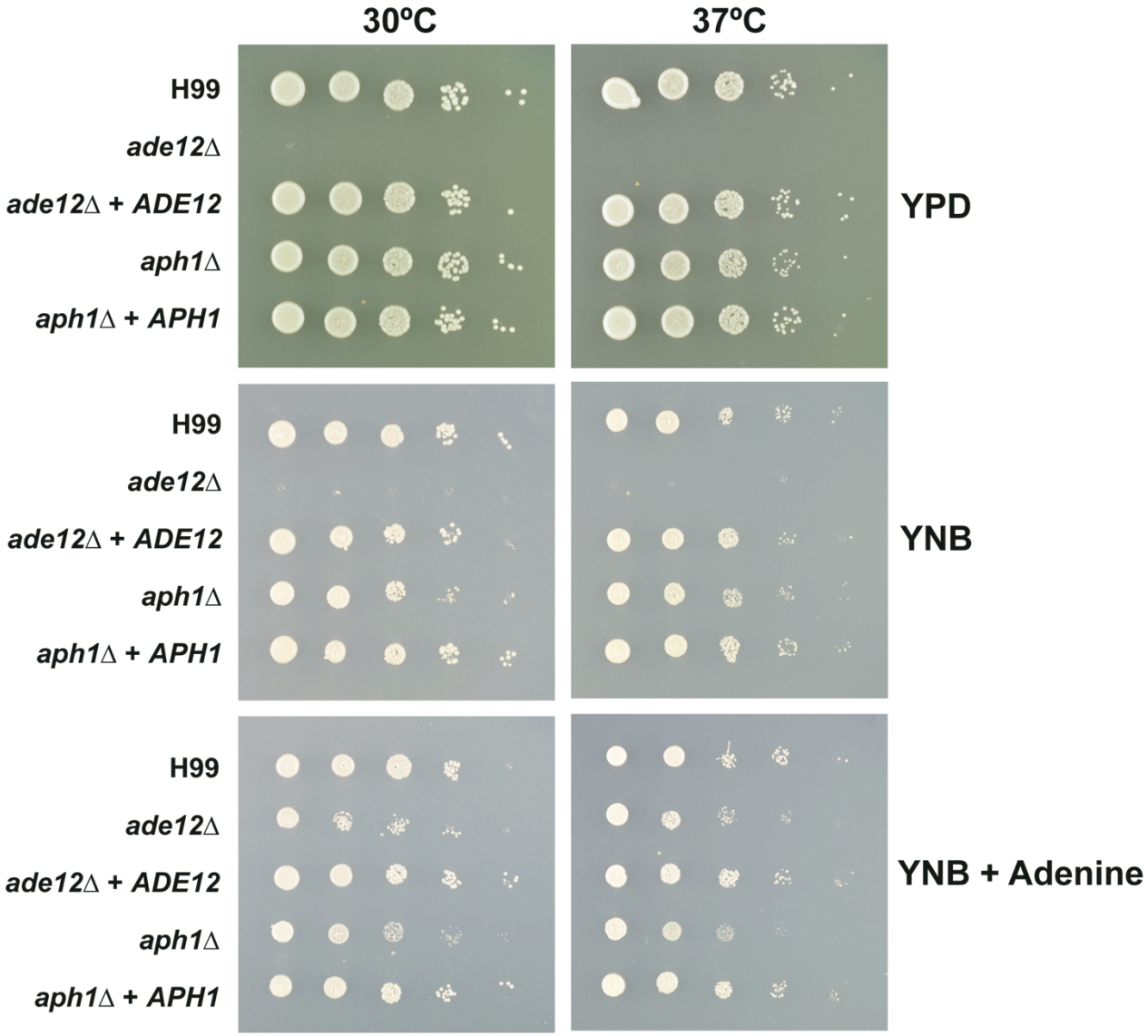

Fig 4*. The loss of AdSS activity results in adenine auxotrophy. 10-fold serial dilutions of the indicated strains were spotted onto either YPD complete media or YNB minimal media supplemented with 2% glucose and 100 mM ammonium sulfate alone, or additionally supplemented with 2 mM adenine. The ade12Δ deletion strain is an adenine auxotroph.*

To confirm that the protein encoded by *ADE12* performed the biochemical functions of the AdSS enzyme, we employed a cross-species complementation approach and introduced *purA*, the AdSS-encoding gene from *E. coli*, into the *ade12*Δ mutant. The *E. coli purA* gene was transformed into the deletion strain under the control of the promoter and terminator regions from *C. neoformans ADE12*. This *ade12*Δ*+PURA* strain displayed a partial complementation of the deletion mutant's adenine auxotrophy (Fig 5). Taken together, these results confirm that the adenine auxotrophy phenotype was due to the loss of AdSS activity.

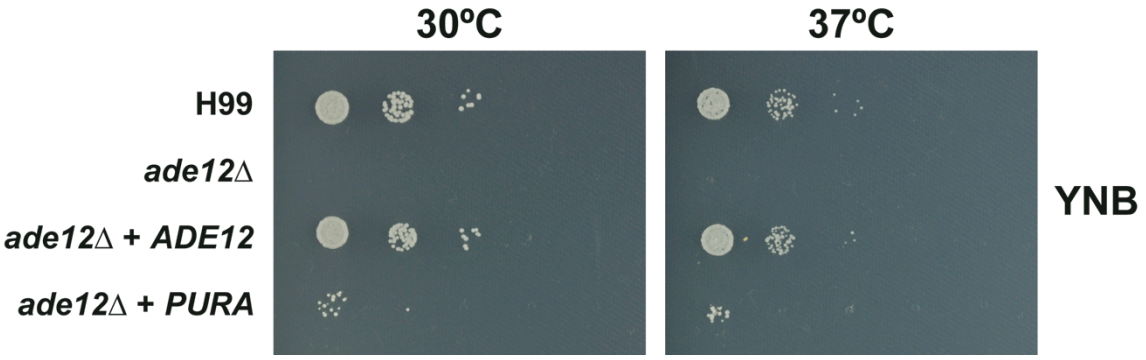

***Fig 5**. Introduction of E. coli ortholog purA partially reverses the adenine auxotrophy of the ade12Δ mutant. 10-fold serial dilutions of the indicated strains were spotted onto YNB minimal media supplemented with 2% glucose and 100 mM ammonium sulfate. The adenine auxotrophy of the ade12Δ mutant is only partially complemented by the E. coli gene.*

Loss of AdSS function does not influence virulence factor production

C. neoformans possesses several virulence factors that help it establish and maintain infection in a human host. Key among these are the polysaccharide capsule, which defends against macrophage attack and opsonization; melanin, which defends the cell from free radicals; urease, which assists with dissemination from the lungs; and the ability to grow at human body temperature.

We investigated the effects of the deletion of the AdSS gene on *C. neoformans* virulence factor production by testing the *ade12*Δ strain and its complemented derivative in a variety of *in vitro* assays. In contrast to changes in virulence factor production described previously in the *imd1*Δ GTP biosynthesis mutant [(31)], *ade12*Δ displayed no defect or delay in any of the phenotypes tested (Fig 6). When grown on l-DOPA media, the deletion strain displayed melanin production comparable to that of the wild-type strain. India-ink staining revealed no significant reduction in the mutant's production of the polysaccharide capsule. *ade12*Δ had no detectable effect on the fungus' response to the cell wall stressors caffeine, calcofluor white and congo red, and there was also no defect in the production of phospholipase B in the deletion strain. Across all tests, *ade12*Δ displayed no defect in growth at 30 or 37 ˚C compared to the wild-type strain.

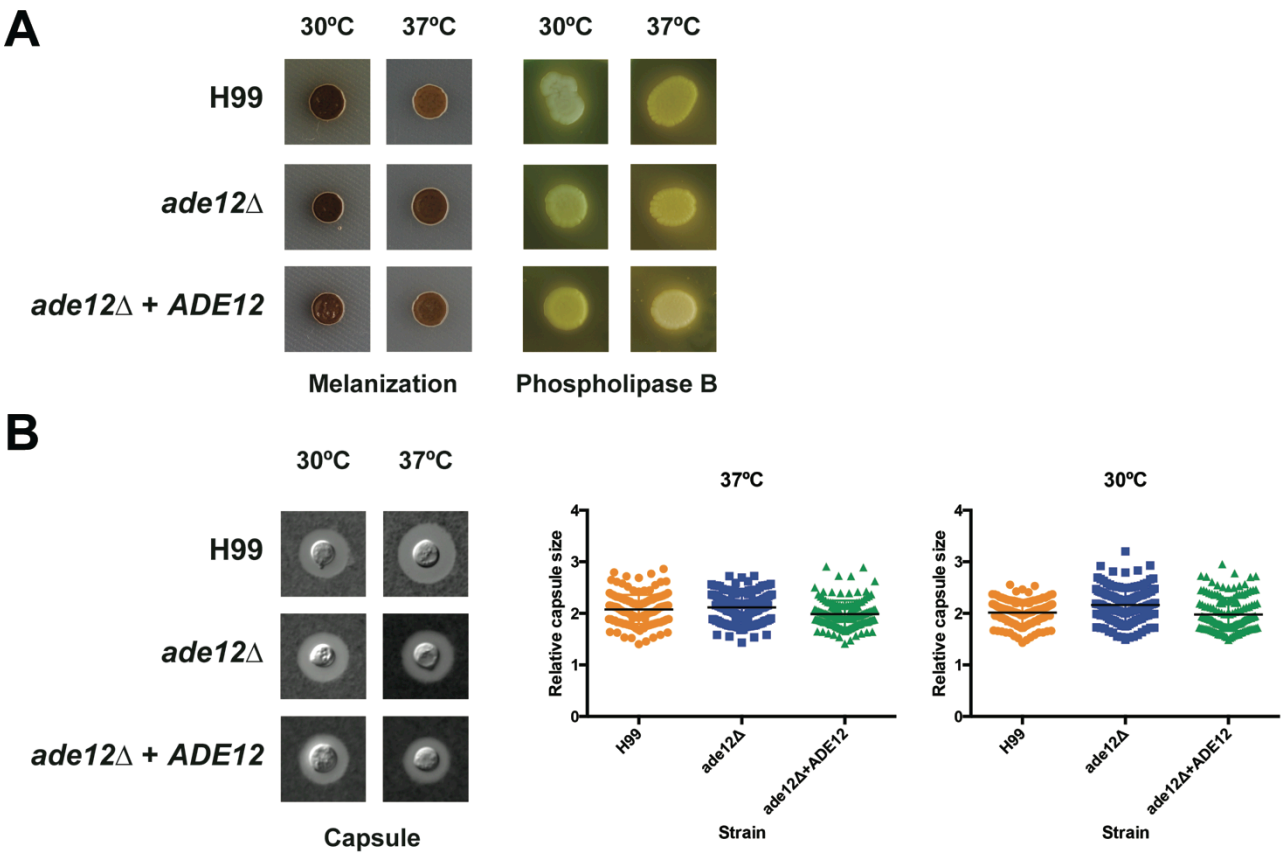

***Fig 6**. Loss of AdSS activity does not impact on virulence factor production. (A) The indicated strains were spotted onto L-DOPA melanization media or egg yolk media and incubated for 48 h at 30 ºC or 37 ºC. (B) The indicated strains were grown in RPMI 1640 media plus 10% BSA and 2 mM adenine at 30 ºC or 37 ºC for 24 h. Capsule was visualized by India-ink staining, and the relative capsule diameter was measured. Cell diameters of mutant and complement strains were compared to the wild-type strain using a 1-way ANOVA with Sidak's multiple comparison post test. No significant reduction of capsule diameter was detected at either temperature tested. A slight increase in capsule diameter was detected in ade12Δ at 30 ºC ($P \leq 0.0001$), and in ade12Δ+ADE12 at 37 ºC ($P \leq 0.01$).*

Identification of the gene required for adenine salvage in *C. neoformans*

In addition to de novo biosynthesis, *C. neoformans* is able to synthesize ATP by another route – it can take up purines from its environment via the purine salvage pathway, and it is through this activity that we can culture the *ade12*Δ mutant in the presence of adenine. To validate the AdSS-dependent de novo synthesis of ATP as a potential target for drug development, we first had to confirm that this alternative mechanism of ATP synthesis was not important during the infection process. Therefore, while characterizing the ATP branch

of the biosynthetic pathway, we also investigated the adenine salvage enzyme adenine phosphoribosyltransferase. The adenine phosphoribosyltransferase-encoding *APH1* gene was identified in the *C. neoformans* genome using reciprocal best-hit BLAST analysis against the orthologous *S. cerevisiae* gene *APT1*. It has the locus number CNAG_01390, is located on chromosome 5 in a single copy and, like *ADE12*, is highly conserved; the predicted product has 51% and 40% identity to the *S. cerevisiae* isoforms 1 and 2 respectively; 46% against the human; and 41% against the *E. coli* enzyme.

Loss of adenine salvage function does not influence virulence factor production

In order to investigate the impact of *APH1* on virulence, we employed biolistic transformation to delete it from the type strain H99, and to complement the deletion mutant with the wild-type gene, creating the strains *aph1*Δ and *aph1*Δ*+APH1*. These strains were created by Adre Koh and Kirsten Blake, respectively.

As expected, *aph1*Δ did not display adenine auxotrophy, with both the deletion and complementation strain able to grow on minimal media without supplementation (Fig 4). The *aph1*Δ strain was also tested for the production of key virulence factors, but was found to be indistinguishable from the wild-type strain under all conditions tested (Fig 7).

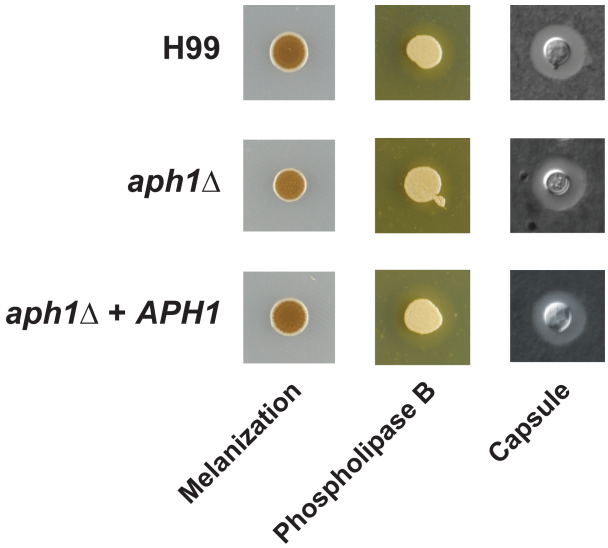

Fig 7: *Loss of adenine salvage does not impact on virulence factor production. The indicated strains were spotted onto L-DOPA melanization media or egg yolk media and incubated for 48 h at 30 ºC. The indicated strains were also grown in RPMI 1640 media plus 10% BSA at 30 ºC for 24 h. Capsule was visualized by India-ink staining,*

Loss of adenylosuccinate synthetase activity renders *C. neoformans* avirulent *in vivo*

The dramatic loss of *in vivo* virulence displayed by IMP dehydrogenase deletion strains [31] makes it clear that *C. neoformans* cannot cause a life-threatening infection without this step of *de novo* GTP biosynthesis. What is not clear is whether this attenuation is due to the mutant's observed delay in virulence factor production, guanine auxotrophy, or a combination of the two.

With AdSS we expected no such ambiguity, as virulence factor production in the *ade12*Δ mutant was not affected. We used the murine inhalation model of cryptococcosis to compare the virulence of the wild-type, *ade12*Δ and *aph1*Δ strains, and their complemented derivatives. Mice infected with the wild-type strain succumbed to infection within 24 days. There was no significant difference between this result and mice infected with the *aph1*Δ deletion mutant, or the *aph1*Δ*+APH1* and *ade12*Δ*+ADE12* complemented strains. In contrast, mice infected with the *ade12*Δ deletion strain remained healthy even up to 32 days post-infection (Fig 8A). Subsequent analysis of fungal organ burden of culled mice revealed that those infected with the wild-type, *aph1*Δ and both complemented strains suffered significant fungal colonization of the lungs and dissemination to all organs tested. Those infected with the *ade12*Δ strain had cleared their infection, with no fungal cells present in any organs tested (Fig 8B). Time-course experiments were conducted to determine whether this effect was truly due to loss of virulence and eliminate the possibility that the infection inoculum were simply not viable without adenine. We found that the *ade12*Δ deletion strain was able to survive for over 9 hours after being transferred from adenine-supplemented to non-supplemented media (data not shown). This is in line with our previous studies in guanine biosynthesis, in which it was found that IMPDH-deficient cells were able to infiltrate from the lungs of infected mice, only to be rapidly cleared [31].

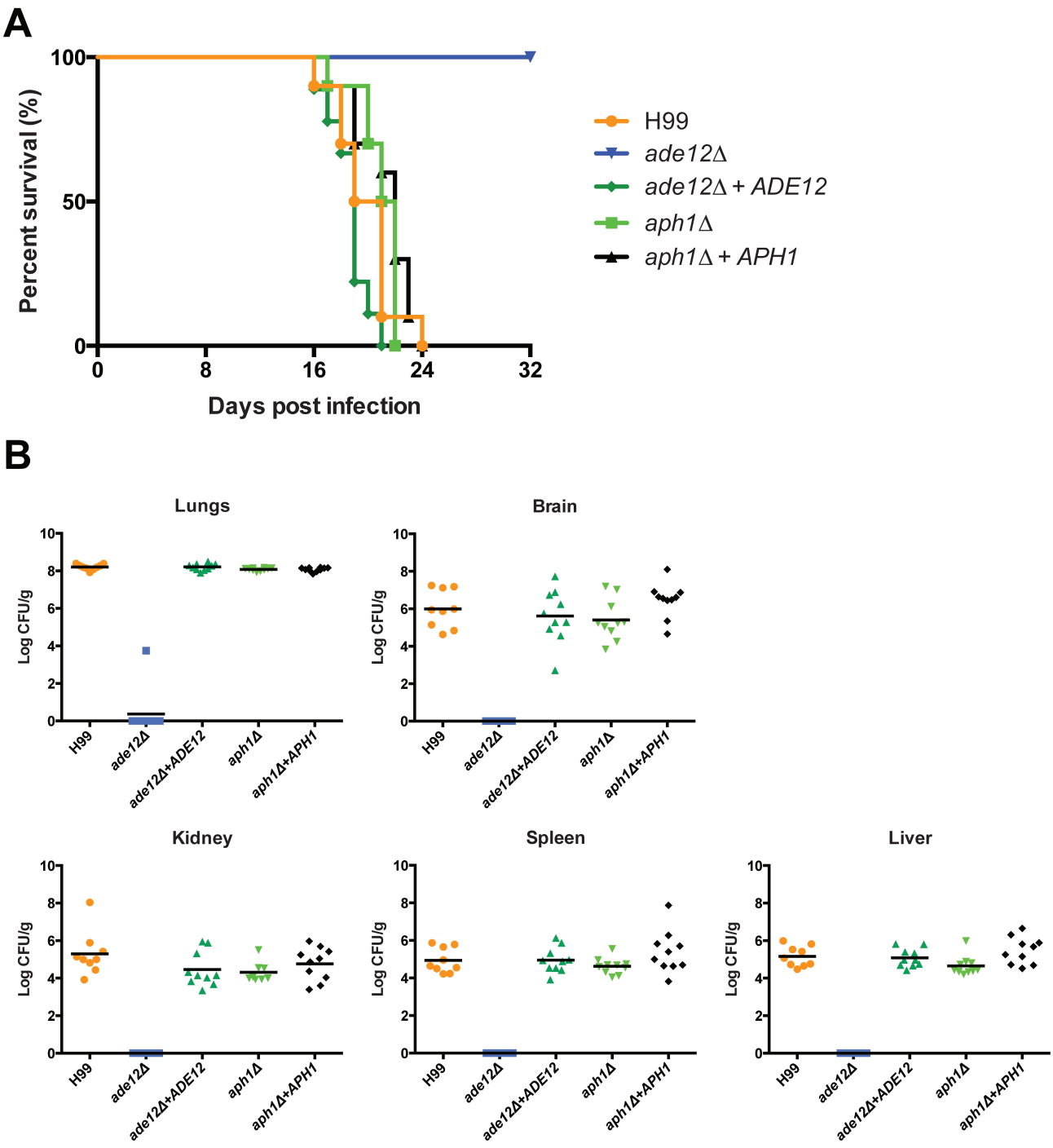

Fig 8. *ADE12 is essential for virulence and dissemination in a mammalian host, while APH1 is not. (A) Survival of female BALB/c mice infected with 5 × 105 cells by nasal inhalation. (B) Fungal burden of organs recovered from infected mice.*

Organ burden of mutant and complement strains was compared to the wild-type strain using a 1-way ANOVA with Sidak's multiple comparison post-test. In all organs tested, ade12Δ was found to be significantly lower ($P \leq 0.0001$). No significant difference was found in any other strain in any organ tested.

The fact that *ade12*Δ, with its fully functioning suite of virulence factors, displayed the same loss of virulence as previously reported for IMP dehydrogenase deletion mutants indicates that this effect is likely mediated solely by purine auxotrophy. Additionally, the adenine salvage pathway was found to be expendable during infection, in line with previous deletion studies in guanine salvage [(31)], again highlighting the importance of de novo purine biosynthesis during the infection process; *Cryptococcus* causes deadly fungal meningoencephalitis after disseminating to the central nervous system, which is relatively poor in purines compared to the fungus' native environment [(32)]. Our data support the model that *C. neoformans* is entirely reliant on its *de novo* purine biosynthesis during infection, as there are insufficient salvageable purines in the cerebrospinal fluid to support growth. If deprived of *de novo* purine synthesis during infection, the production of virulence factors would be irrelevant, as the fungus would be unable to grow at all. This represents a fundamental and potentially crippling vulnerability within the fungus, one that should be exploited through rational drug design.

Steady-state enzyme kinetics of cryptococcal AdSS

The development of targeted antimicrobial drugs requires an established assay with which to assess the activity of new compounds. Furthermore, insights into the kinetic parameters of the target enzyme are required to characterize the mechanism of action by possible drug candidates. Differences in the kinetic parameters between orthologous enzymes may also indicate potentially exploitable mechanistic differences or structural features. In the case of AdSS, the conversion of IMP and l-aspartate to adenylosuccinate proceeds via two steps, as confirmed and exemplified by the well-studied AdSS enzyme in *E. coli* [(89)]. In the first step, the γ-phosphate from GTP is transferred to the 6-oxygen of IMP. This forms the intermediate 6-phosphoryl IMP (6-PIMP) with the 6-phosphoryl group then displaced by the α-amino group of aspartate to form adenylosuccinate (Fig 9A).

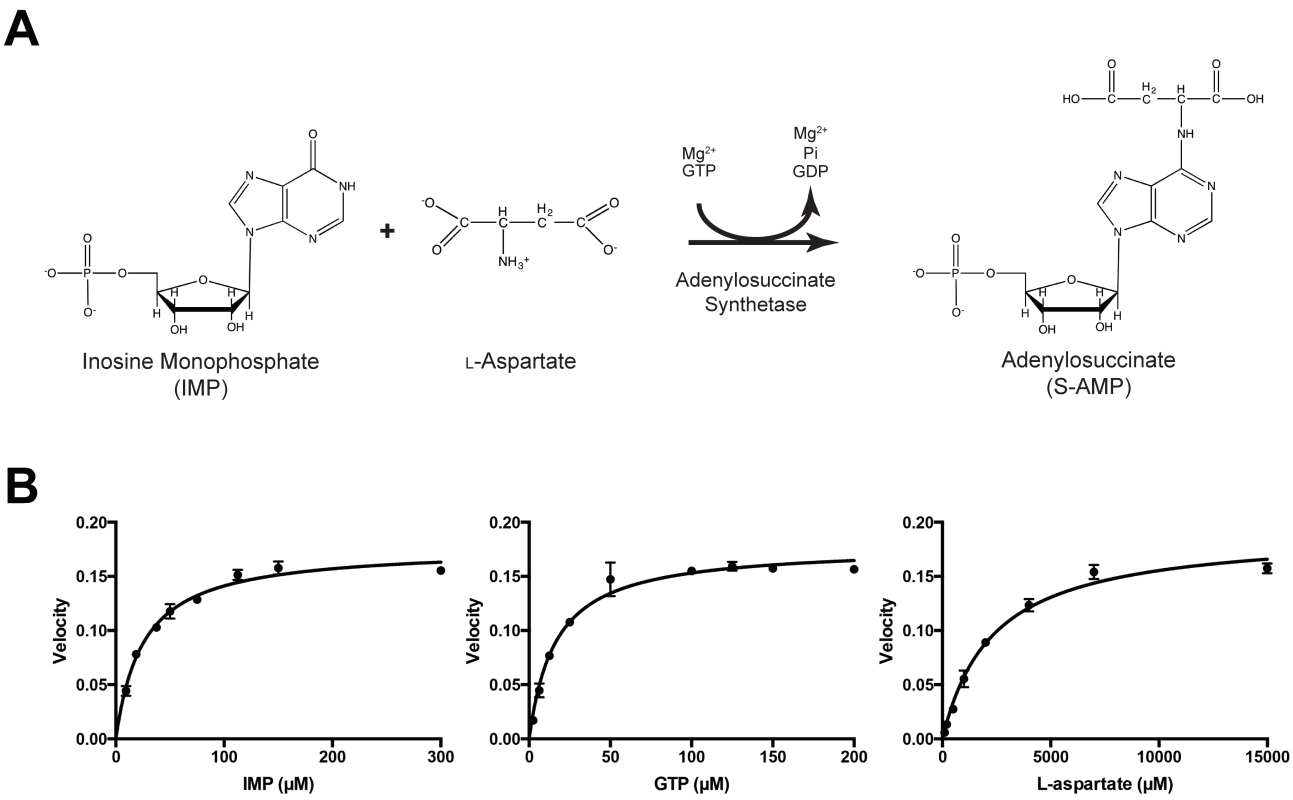

***Fig 9**. Enzyme kinetics of C. neoformans AdSS. (A) AdSS enzyme reaction scheme. (B) Substrate concentration (μM) vs enzyme velocity (∆Abs/min), with non-linear fitting of Michaelis-Menten equation.*

In order to characterize this reaction in the *C. neoformans* enzyme, we created a gene construct that contained an N-terminal 6×His-tag fused to the *C. neoformans* AdSS. This tagged enzyme was expressed in *E. coli* and purified the protein by nickel affinity and size-exclusion chromatography [(80)]. Pure recombinant *C. neoformans* AdSS was used to determine the steady-state parameters of the enzyme (Fig 9B). The purified enzyme was enzymatically active, as shown by an increase in adenylosuccinate specific absorption at 280 nm. Cryptococcal AdSS displayed a relatively high k_{cat} of 3.21s-1, between 3- and 5-fold higher than reported in other species (Table 1). This may explain why complementation with the *E. coli* enzyme only partially reversed the auxotrophy of the *ade12*∆ strain.

***Table 1**. Comparison of reported kinetic paramaters of AdSS from multiple species.*

Species	**k_{cat} (S^{-1})**	**K_M IMP (μM)**	**K_M GTP (μM)**	**K_M aspartate (μM)**
C. neoformans	3.21	25.30 ± 1.8	16.3 ± 1.3	2330 ± 197
S. cerevisiae [88]	0.2	200 ± 18	81	1650
P. falciparum [90]	N/A	22.8	4.8	1400
E. coli [43]	0.59	21 ± 2	22 ± 5	280 ± 40
M. musculus muscle [50]	1.0	45 ± 7	12 ± 2	140 ± 15
H. sapiens muscle [91]	0.2	N/A	N/A	N/A

The *C. neoformans* enzyme also exhibited a very high K_M for aspartate (2330 ± 197 μM), a trait shared with enzymes from *S. cerevisiae* and *P. falciparum*, but not the bacterial or mammalian orthologs. The reported IMP and GTP K_m values for the *S. cerevisiae* enzyme are approximately 8-fold higher than those from *C. neoformans* (25.3 ± 1.8 μM for IMP, 16.3 ± 1.3 μM for GTP), which are more in line with those reported for *E. coli* AdSS (Table 1). Unfortunately, little work towards characterizing human AdSS has been reported, making direct comparison of K_M values impossible. The AdSS muscle isozyme from mice has been characterized, with a 55% higher K_M for IMP than the *C. neoformans* enzyme and an equivalent K_M for GTP.

An existing AdSS inhibitor exhibits limited antifungal activity

When searching for antimicrobial compounds, finding an already well-established drug that is active against a new organism of interest can be a significant advantage, as synthesis methods, commercial stocks or even clinical trial data may already be available. AdSS currently has a limited number of well-characterized inhibitors, including the antibiotic l-aspartate analogue hadacidin [60]. We determined whether this compound was capable of recreating the *ade12*Δ auxotrophy phenotype in a range of pathogenic fungi.

We assayed the minimum inhibitory concentration of hadacidin in adenine-free media against a panel of six fungal strains: two *C. neoformans* isolates, as well as *C. albicans*, *C. parapsilopsis*, *C. glabrata* and *A. fumigatus*. Fungal cells were exposed to increasing concentrations of hadacidin to determine minimum inhibitory concentration for each strain. The concentrations tested – a 12-step, 2-fold serial dilution starting at 0.1 mg/mL (168 μM)

and ending at 0.5 µg/mL (4 µM) – were chosen based on previously reported *in vivo* experiments (32), as well as limited compound availability.

We found that only one assayed combination exhibited any change in fungal growth; 168 µM hadacidin, the highest concentration tested, lead to reduced growth of *C. albicans*. OD_{600} of the treated assay condition at 72h dropped to an average value of 0.877 compared to 0.995 in the adjacent condition treated with 84 µM hadacidin and 1.085 in the untreated condition. No other strains, including both *C. neoformans* isolates, exhibited any inhibition of growth when exposed to the drug.

The lack of even moderate antifungal activity of hadacidin against *C. neoformans* could easily be explained by either poor compound entry into the cell, or insensitivity of the enzyme to this inhibitor. To determine whether hadacidin was active against the cryptococal enzyme despite having no anticryptococcal activity at the concentrations tested, we determined the IC50 value of the compound against purified *C. neoformans* AdSS in our *in vi*tro assay.

50% reduction in reaction velocity was found to occur at 255 µM, a concentration that exceeds the highest tested in our MIC assays. Other potential factors, including degradation of hadacidin in the media and problems with uptake into the cytoplasm, could also have lowered the functional concentration in the fungal growth inhibition MIC assay further. Furthermore, during the IC50 determination, we found that the rate of decrease of AdSS velocity with respect to hadacidin concentration followed an exponential decay curve that plateaued at 30% remaining activity (Fig 10). This indicates that hadacidin would likely be unable to fully inhibit the activity of *C. neoformans* AdSS, even at millimolar concentrations. In light of these results, it is also reasonable to conclude that hadacidin is not an inhibitor of *C. neoformans* AdSS under these conditions

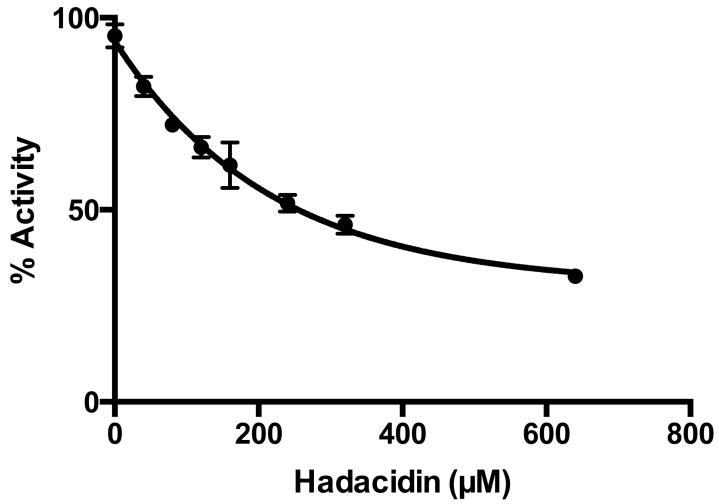

Fig 10. *Hadacidin could not fully inhibit C. neoformans AdSS activity. Hadacidin concentration (μM) vs percent enzyme activity with non-linear fitting of single-phase exponential decay equation.*

Chapter 4: AdSS crystallization

This paper was submitted to Acta Crystallographica Section F (Structural biology and crystallization communications), and published in 2013. It encompasses my efforts to express and purify *C. neoformans* AdSS in *E. coli*, optimize conditions for crystallizing AdSS, and the preliminary analysis of X-ray diffraction data obtained from the resulting crystals. For brevity and convenience, references to figures and tables in the originally published paper have been altered to refer to equivalent figures and tables reported elsewhere in this manuscript where possible, and the original paper's reference list has been incorporated into this manuscript's reference section.

I completed the experimental work (90%) with some preliminary preparation performed by Carl Morrow (5%). I performed the data analysis (70%) with assistance from Simon Williams (20%) and Daniel Ericsson (10%). I designed the experiments (80%) with assistance from Simon Williams (20%). I wrote the text of the paper (85%) with drafting assistance from James Fraser, Bostjan Kobe, and Simon Williams (5% each).

Purification, crystallization and preliminary X-ray analysis of adenylosuccinate synthetase from the fungal pathogen *Cryptococcus neoformans*

Ross D. Blundell[a], Simon J. Williams[a,b], Carl A. Morrow[a], Daniel J. Ericsson[a,b]

Bostjan Kobe[a,b]* and James A. Fraser[a]*

[a]Australian Infectious Diseases Research Centre,

School of Chemistry and Molecular Biosciences,

The University of Queensland, Brisbane, QLD 4072 Australia

[b]Institute for Molecular Bioscience,

The University of Queensland, Brisbane, QLD 4072 Australia

Introduction

With the rise of the HIV/AIDS pandemic and the increased use of immunosuppressive drugs in chemotherapy and organ transplantation, populations of individuals with defective immune systems are higher than ever before. With such a large immunocompromised population, opportunistic infections are a growing cause of morbidity and mortality. Among these opportunists is the fungus *Cryptococcus neoformans*, one of the foremost AIDS-defining illnesses. Infection by this basidiomycete yeast begins with inhalation of spores or desiccated yeast cells [(92)]. Individuals with healthy immune systems generally clear infection by *C. neoformans*. However, in immunocompromised individuals, the fungus can disseminate to the central nervous system to cause cryptococcal meningoencaphalitis, which is fatal if untreated [(92)].

Fungal infections are difficult to treat due to the similarities of their eukaryotic physiology to that of humans; the limited antifungal agents available tend to target the few differences between the two systems [(16)]. Azoles (such as fluconazole) and polyene compounds (such as amphotericin B) target ergosterol by inhibiting the enzyme involved in its biosynthesis (lanosterol 14 α-demethylase), or by binding to ergosterol itself, respectively. New agents of this class are frequently reported, however few see active clinical development [(19)]. Sordarins, which inhibit protein synthesis via elongation factor 2 [(27)] and echinocandins, which inhibit fungal cell wall glucan synthesis [(93)], both show promise as antifungal agents, but few specific candidates for further trials have emerged [(19)] Considering the current shortage of new drug candidates in the antifungal pipeline, the discovery and development of novel fungal-specific compounds needs to be given a high priority. One approach to achieve this is to apply rational drug design techniques towards fungal-specific aspects of otherwise conserved metabolic pathways.

The purine metabolic pathway has for over half a century served as a source of targets for therapeutic compounds including antitumor drugs, immunosuppressants and antivirals [(28)]. Previous studies by our group have shown that purine metabolism is a potential source of antifungal drug targets to combat *C. neoformans* infection [(31, 33)]. We have already characterized a crucial enzyme in the purine biosynthesis pathway in this organism, inosine monophosphate dehydrogenase (IMPDH). IMPDH is the first committed step in *de novo* GTP biosynthesis, catalyzing the conversion of inosine monophosphate (IMP) to xanthosine monophosphate (XMP). Loss of IMPDH activity, and consequently *de novo* GTP biosynthesis, results in the death of the pathogen, suggesting that this pathway may

be a viable antifungal target [31]. To further probe this pathway for targets, we have investigated other purine biosynthetic enzymes.

Just as IMPDH catalyzes the first step in GTP biosynthesis from IMP, the first step in the conversion of IMP to ATP is governed by the enzyme adenylosuccinate synthetase (AdSS). AdSS catalyzes the formation of adenylosuccinate (s-AMP) from IMP and aspartate. This GTP and Mg^{2+} dependent reaction proceeds via two steps: firstly, the γ-phosphate from GTP is transferred to 6-oxygen of IMP, forming the intermediate 6-phosphoryl IMP (6-PIMP); secondly, the 6-phosphoryl group is displaced by the α-amino group of aspartate to form adenylosuccinate [39] (Fig 9A). Structural studies in *Escherichia coli* and other organisms have shown that the enzyme forms a dimer, with each subunit contributing an arginine residue to the active site of the other molecule [40, 41, 47, 48]. In the absence of its substrate, the active site of AdSS is disordered, however upon ligand binding, the substrate binding pocket and dimer formation are stabilized [44, 94].

With the exception of mature red blood cells, AdSS is an essential enzyme in all organisms studied so far and most cell types, [44, 95]. An alternative route of ATP biosynthesis is the conversion of adenine salvaged from the environment to adenosine monophosphate (AMP). This reaction is governed by the enzyme adenine phosphoribosyl transferase (APRT), which has been characterized in several organisms including the fungus *Saccharomyces cerevisiae* [96]. *C. neoformans* carries a predicted APRT-encoding gene (strain H99; CNAG_02858, Broad Institute of MIT and Harvard; www.broadinstitute.org/annotation/genome/cryptococcus_neoformans/MultiHome.html).

AdSS has been purified and characterized from several sources. AdSS from *E. coli* is arguably the best characterized [41, 97, 98] and has 42% identity with the cryptococcal enzyme. Crystal structures are also available for the proteins from *Homo sapiens* (54%, PDB ID: 2V40); *Mus musculus* (54%, [50, 99]); the bacteria *Yersinia pestis* (42%, PDB ID: 3HID), *Campylobacter jejuni* (43%, PDB ID: 3R7T) and *Burkholderia thailandensis* (40%, PDB ID: 3UE9); the plants *Arabidopsis thaliana* (55%) and *Triticum aestivum* (53%, [49]); the eukaryotic parasite *Plasmodium falciparum* (46%[48]; and the extremophile archaeon *Pyrococcus horikoshii* (33%, [100]). The enzyme has been crystallized in the apo-form [41, 50] as well as complexed with various combinations of IMP, GTP, GDP, aspartate, 6-PIMP, Mg2+, and two AdSS inhibitors: the anti-tumor aspartate analogue hadacidin [56, 61] and the adenosine 5'-monophosphate-mimicking herbicide hydantocidin [63].

To date, there has been no crystallographic studies of AdSS from a fungal species. In the hope that comparison of a fungal AdSS structure with the comprehensive knowledge available from other species may prove useful in the design of future fungal-specific agents, here we describe the crystallization and initial analysis of the crystals of adenylosuccinate synthetase from *C. neoformans*.

Materials and methods

Cloning

Total RNA was isolated from *C. neoformans* var. *grubii* strain H99 using TRIzol (Invitrogen). Intron-free cDNA was then synthesized using a Bioline cDNA synthesis kit (Bioline). The AdSS-encoding gene *ADE12* (strain H99; CNAG_02858, Broad Institute of MIT and Harvard; www.broadinstitute.org/annotation/genome/cryptococcus_neoformans/MultiHome.html) was PCR-amplified, with unique restriction sites (BamHI and PstI) introduced via the specifically designed primers UQ2259 (ACGCACGGATCCATGGCTCCATCCCCGGAGGGA) and UQ2260 (GAACGTCTGCAGTTAGAAGATGATAACGTTCTG). The PCR product was then cloned into the TOPO pCR2.1 vector (Invitrogen), sequenced and ligated into BamHI/PstI-cut pQE-30 expression vector (Qiagen), which introduced an N-terminal 6×His tag (MRGSHHHHHHGS).

Expression and purification

Early failed cloning efforts strongly suggested that the *ADE*12 pQE construct was toxic in *E. coli*. The ligation was therefore transformed into competent BL21(DE3)pLysS *E. coli* cells (Promega) expressing the pREP4 repressor plasmid. Transformed cells were grown in terrific broth (TB) media with 100 µg/mL ampicillin, 35 µg/mL kanamycin and 12.5 µg/mL chloramphenicol. Cultures were incubated at 310 K until they reached an OD_{600} of approximately 1.0, after which they were induced with 1 mM IPTG and grown at 293 K for 5 hours. Cell pellets were harvested and resuspended in lysis buffer (50 mM HEPES pH 8, 300 mM NaCl, 1 mM DTT, 30 mM imidazole, and 1 mM PMSF) then lysed by sonication. AdSS was purified via Ni-immobilised metal-affinity chromatography using HisTrap fast flow columns (GE Healthcare) and eluted over 20 column volumes in a linear gradient of 30-500 mM imidazole. A single main elution peak was seen. Fractions corresponding to this peak were combined and further separated over a Superdex 200 size-exclusion

chromatography (SEC) column (GE Healthcare) equilibrated in SEC buffer (10 mM HEPES ph7.5, 150 mM NaCl, 1 mM DTT) using an ÄKTA-Purifier FPLC system (GE Healthcare). Peak fractions were combined and concentrated to approximately 16 mg/mL at >99% purity estimated by Coomassie-stained SDS-PAGE gel and snap-frozen for storage at 193 K.

Crystallization

All crystallization experiments were performed using the hanging drop vapor diffusion method at 293 K. Initial screening for crystallization conditions was performed using the Index and Peg/Ion (Hampton Research), Pact Premier and JCSG (Qiagen), Proplex and Morpheus (Molecular Dimensions), and Synergy (Jena Biosciences) commercial screening plates. Plates were set up by a Mosquito Nanodrop crystallization robot (TTP LabTech), with each drop containing 100 nL protein solution and 100 nL reservoir solution inverted over reservoirs of 100 µL. A Rock Imager system (Formulatrix) was used to monitor crystal growth in the drops. Crystals were found in approximately 200 conditions. The most promising candidates were chosen for further screening and optimization. Final diffraction-quality crystals were obtained using a condition from the PACT screen. Drops containing 1 µL of protein solution at 16 mg/mL and 1 µL of reservoir solution (0.1 M BisTris propane pH 8, 0.2 M sodium bromide, 17% polyethylene glycol 3350) were streak-seeded from non-suitable AdSS crystals after 30 minutes equilibration over 500 µL reservoirs. Long rectangular crystals of approximately 0.5 × 0.05 × 0.05 mm formed after 24-48 hours (Figure 2).

Data collection and processing

Crystals were mounted on nylon loops and treated with a cryoprotectant before being flash-cooled in liquid nitrogen. Initial tests using 20% glycerol in crystallization solution caused crystals to shatter, so 15% ethylene glycol was used as a cryprotectant. X-ray diffraction was performed on the MX2 beamline at the Australian Synchrotron (Clayton, Australia). Reflections were indexed and integrated using the program *XDS* [(101)] then scaled using *Aimless* as implemented within the CCP4 suite [(82)]

Results and discussion

Full-length His-tagged AdSS from *C. neoformans* was expressed heterologously in soluble form in *E. coli* after 5 hours induction at 293 K. Protein appeared as a single band of approximately 46 kDa on reducing SDS-PAGE gels, matching the estimated size of His-tagged AdSS. During SEC, the protein elutes at 220 mL, which, based on its expected molecular weight and protein calibration standards, suggests a monomeric state in solution. This is in keeping with the established model in which AdSS dimerization is dependent on ligand binding [(46)].

Following the large number of hits obtained from initial sparse-matrix screening, trends in crystallization conditions were investigated. Many hits occurred in conditions using PEG3350 as a precipitant with various types of salts. After comparing the morphologies of these hits, a buffer containing PEG3350 and sodium bromide was chosen. Further rounds of optimization by varying pH, PEG concentration, and the addition or absence of glycerol led to large, diffraction quality crystals in 0.1 M BisTris propane, pH 8, 0.2 M sodium bromide and 17% polyethylene glycol 3350. Protein crystals appeared after 24-48 hours at 293 K (Fig 11). The resolution of the best-diffracting crystals was 2.2 Å. Data collection and refinement statistics are summarized in Table S3. The crystals most likely contain 2 molecules in the asymmetric unit (corresponding to the Matthews coefficient of 2.61 $Å^3$/Da) [(102)].

Current work is focusing on solving the structure of AdSS by molecular replacement based on the most similar crystallized homologue (*A. thaliana*) as well as obtaining datasets for ligand- and inhibitor-bound forms. Analysis of these structures may reveal differences from the human enzyme that could be exploited by structure-based inhibitor design to create leads for new antifungal therapeutics.

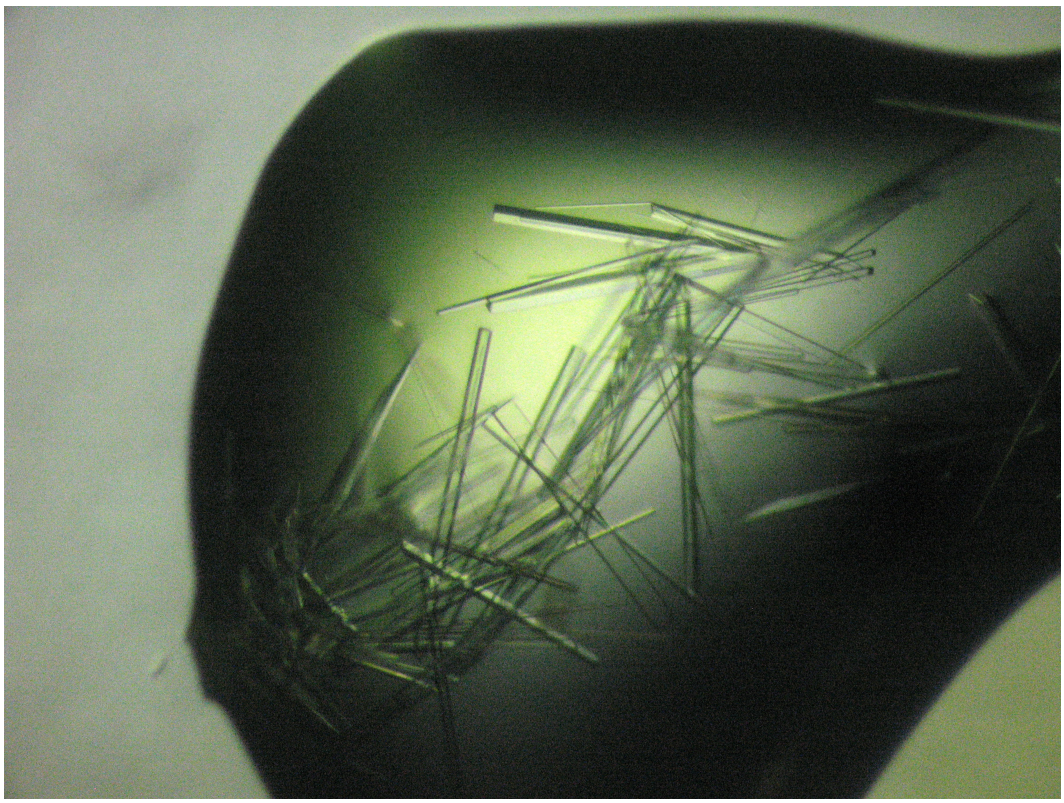

***Fig 11**, Crystals of adenylosuccinate synthetase from C. neoformans, space group $P2_12_12_1$.*

Chapter 5: AdSS apoenzyme.

Crystal structure of unligated cryptococcal AdSS

To enable comparisons between the *C. neoformans* enzyme and those from other species, and identify targetable species-specific features, we determined the crystal structure of the *C. neoformans* AdSS apo-enzyme to 2.2 Å resolution. The *C. neoformans* AdSS structure contained two molecules within the asymmetric unit, which resembled the functional homoodimer observed in other AdSS crystal structures (Fig 12A). The overall structure of the enzyme was very similar to the well-characterized *E. coli* AdSS (PDB ID: 2GCQ) with an overall root-mean-square deviation (RMSD) of 1.30 Å across 378 residues. Of the 430 residues in the *C. neoformans* sequence, only 388 could be modelled in each chain, as regions corresponding to residues 51-58, 122-141, 171-194 were disordered. These missing residues corresponded to the flexible active site loops described in other species [(41)], which only become ordered in these species when the enzyme is fully ligated.

Confirmation of AdSS dimerization

To confirm the homodimeric AdSS arrangement seen in our crystal structure, we used Size exclusion chromatography linked to multi-angle light scattering (SEC-MALS) to determine the molecular weight of our purified AdSS in solution. The monomeric molecular weight of the recombinant AdSS protein is ~48 kDa, while the measured molecular weight analyzed by SEC-MALS is ~97 kDa (Fig 12B), consistent with the protein forming a stable dimer. AdSS dimerization is stabilized by the binding of IMP, and our SEC-MALS analysis was performed without ligands. However, AdSS dimerization in physiological concentrations is governed by an equilibrium between monomer and dimer, an equilibrium that substrate binding tips towards the dimer. Because the standard enzyme concentrations used in our SAX-MALs experiments were approximately ten times above the dimer's dissociation constant in other species [(46)], the dimerization of the *C. neoformans* apoenzyme is most likely the result of this elevated concentration allowing the enzyme to dimerise without substrates.

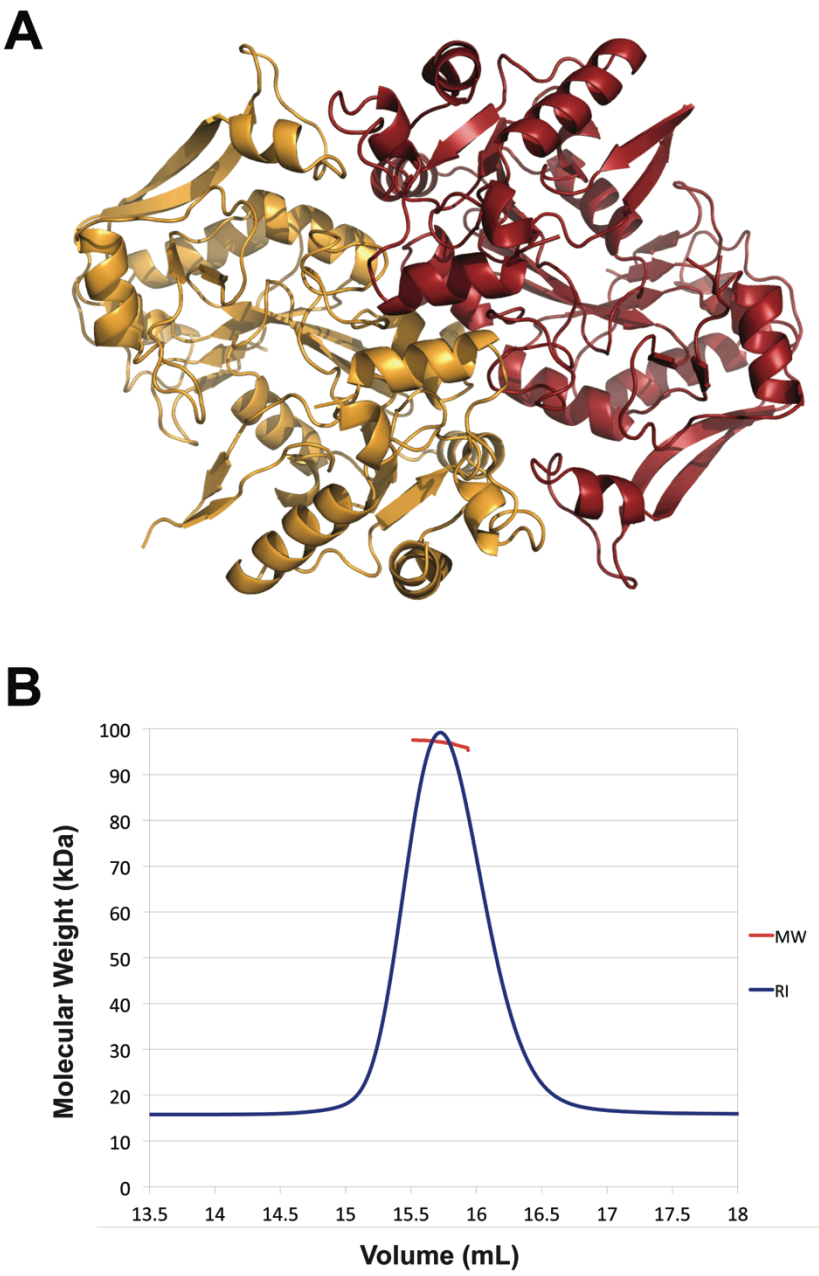

***Fig 12**. Crystal structure of apo-AdSS. (A) Crystal structure of C. neoformans AdSS dimer (shown in cartoon form). Gold and red indicate separate monomers. (B) SEC-MALS analysis of AdSS. The blue line indicates the trace from the refractive index detector (arbitrary units) during SEC. The red line indicates the molecular weight (Y- axis) determined by MALS, distributed across the SEC peak.*

Chapter 6: Ligated AdSS enzyme

Crystal structure of ligated cryptococcal AdSS

In order to obtain a more complete C. neoformans AdSS model and better facilitate accurate comparison of the fungal enzyme to structures from other species, we set up co-crystallization experiments whereby IMP, GTP, magnesium acetate and the aspartate analogue hadacidin were all included. The corresponding structure was determined to a resolution of 1.55 Å (Fig 13), a significant improvement in resolution and general B-factors (reflecting the mobility of the atoms, with higher numbers corresponding to higher mobility) over the structure of the apoenzyme (Fig 14). The ligated structure was a homodimer, with 429 of the 430 expected residues in chain A and 413 of 430 residues in chain B. IMP is clearly resolved in the active site of each subunit, with B-factors ranging from 13 to 41 $Å^2$ in chain A, and 12 to 38 $Å^2$ in chain B. Instead of GTP, the hydrolyzed form GDP is found in both active sites, with B-factors ranging from 15 to 21 Å2 in Chain A, and 14 to 38 $Å^2$ in Chain B (Fig 15). Hadacidin was not apparent in its expected binding location despite being present in 10-fold molar excess during crystallization. Along with the apo-AdSS structure produced initially, this represents the first example of an AdSS crystal structure solved from a fungal species.

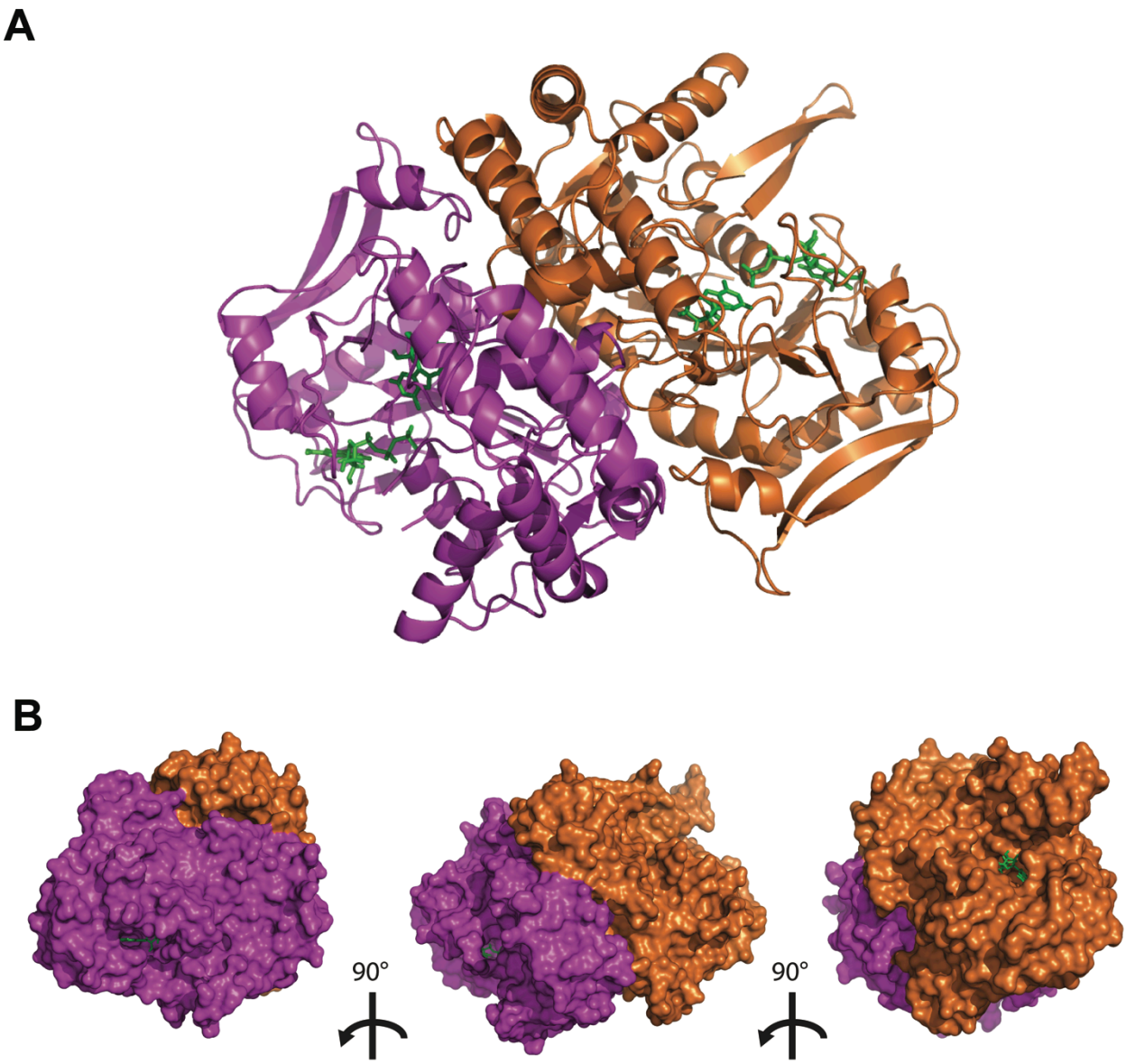

***Fig 13**. Crystal structure of IMP- and GDP-bound AdSS. (A) Crystal structure of C. neoformans AdSS dimer (shown in cartoon form) bound to IMP and GDP. Orange and magenta indicate separate monomers. Bound ligands IMP and GDP are shown in stick form, colored green.(B) Surface mesh of AdSS dimer rotated clockwise in 90º increments to display the active-site clefts. IMP and GDP are shown in stick form, colored green*

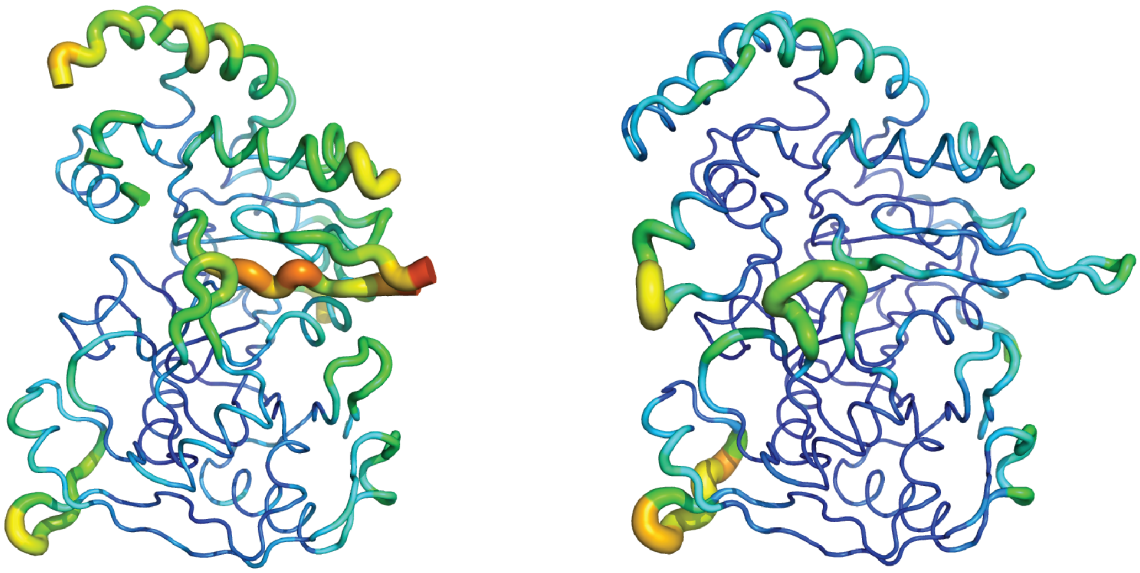

Apo-cnAdSS ***Ligand-bound cnAdSS***

Fig 14*, B-factor putty diagram comparison of apo- and ligand-bound structures of C. neoformans AdSS. Warmer colours and wider tubes indicate higher B-factors, while cooler colours and narrow tubes indicate lower B-factors. Images are viewed at the same orientation, highlighting improvement in B-factors in the ligand-bound structure.*

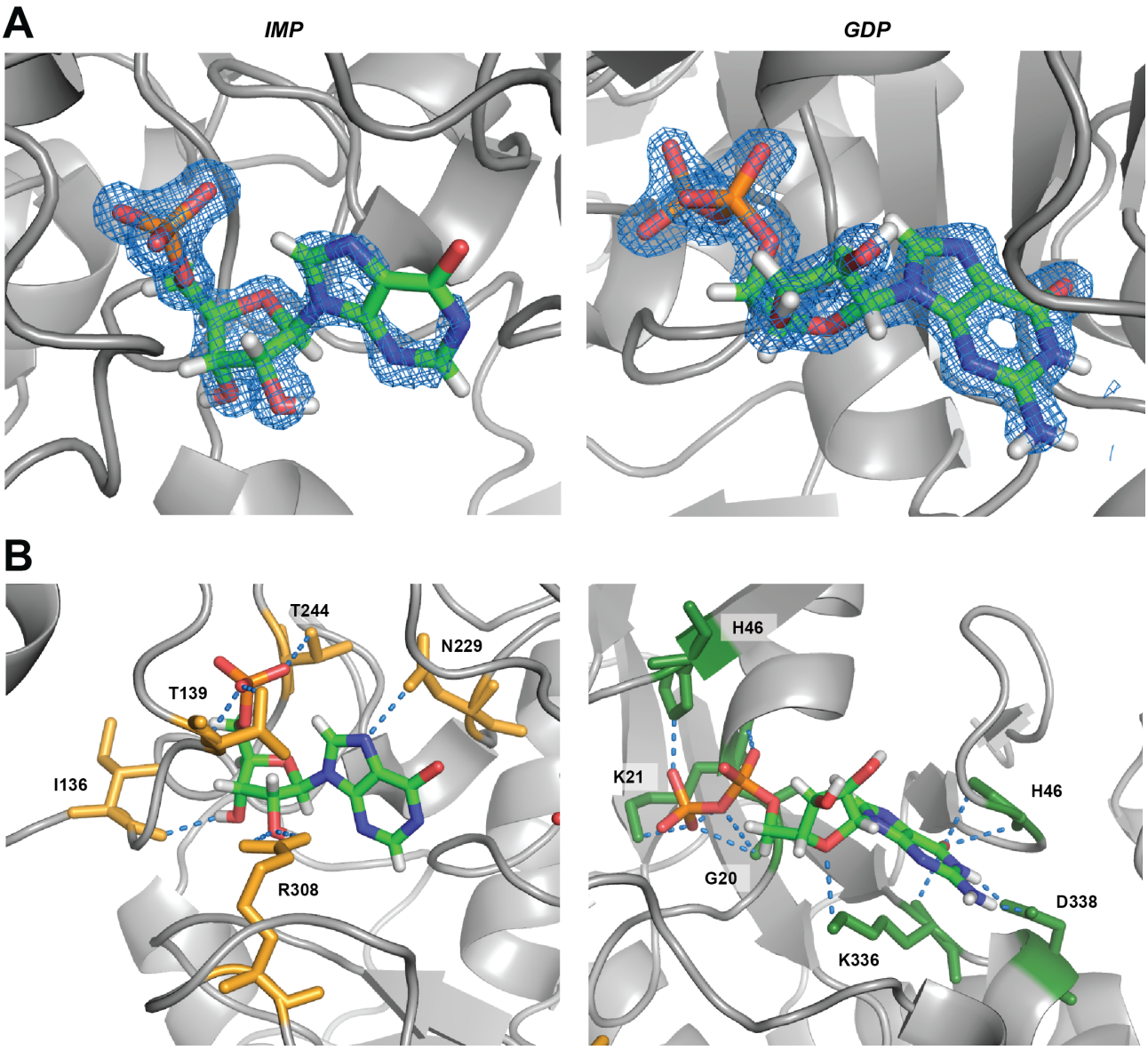

***Fig 15**, IMP and GDP are clearly resolved in the ligated AdSS structure. (A) Fourier map overlay of ligands, indicating electron density at each ligand location. Contour of maps is 2.0 sigma, radius 1.6 Å. (B) Hydrogen bonds between ligands and indicated protein side-chains. All images created using Chain A of the AdSS homodimer.*

As with the structure of the apo-enzyme, the fold of the ligated enzyme resembles that seen in other AdSS proteins. A central core comprised of a twisted nine-strand β-sheet is surrounded by three domains, all combining to form a cleft in which the predicted active site is located (Fig 8B). The most dramatic divergence from the common fold is the β-sheet referred to as B2 in *E. coli*. This sheet is longer in chain A of the ligated *Cryptococcus* structure, corresponding to a 5-residue insertion at the tip of the β-sheet that is not conserved in any other species (Fig 16). This extended β-sheet is on the opposite side of

the structure from the dimerization surface, but is adjacent to the GTP-binding site. In chain B, the entire B2 sheet is unresolved.

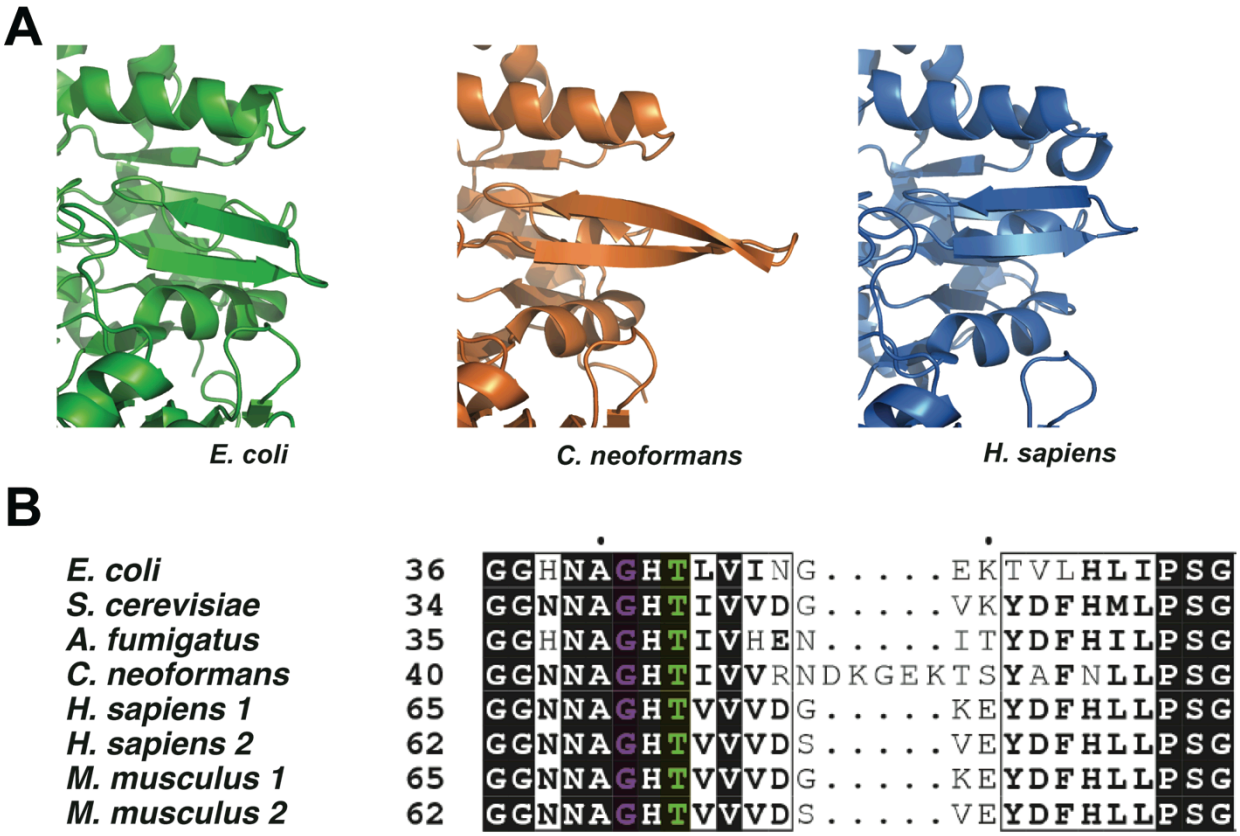

***Fig 16**. C. neoformans AdSS contains an extended B2 β-sheet. (A) Comparison of the B2 β-sheet from E. coli (green, left), C. neoformans (orange, center) and H. sapiens (blue, right) AdSS. The structures are shown in cartoon representation. The PDB IDs for the E. coli, C. neoformans and human structures are 2GCQ, 5I34 and 2V40 respectively. (B) Alignment of B2 β-sheet sequence from multiple species, with general conservation of residues annotated in black, GTP-binding residues annotated in green and magnesium-binding residues annotated in purple. The C. neoformans enzyme contains a 5-residue extension found in no other species examined.*

Comparison of *C. neoformans* and human AdSS active sites

In order to detect exploitable species-specific structural features in the fungal AdSS structure, we compared the active site region of our crystal structure with that from the human AdSS structure (PDB ID 2V40). This structure has been deposited in the PDB archive, but has not yet been described in a dedicated publication. It was crystallized in combination with GDP, which is well resolved in its active site with B-factors of individual atoms ranging from 18 to 27 Å2.

Pairwise structural alignment of the ligand-bound *C. neoformans* and human AdSS structures returns a close match, with an RMSD of 1.16 Å across 408 residues. The human structure contains one gap in visible residue coverage, stretching between residues 150-163. This gap corresponds to the active site loop associated with IMP, consistent with the previously reported requirement of IMP binding for a fully ordered active site and the lack of bound IMP in this structure. The lack of density for this loop means that the IMP-binding site is incomplete, rendering a complete comparison of this site between the human and *C. neoformans* AdSS enzymes impossible.

Partial comparisons can be made, however. In the *C. neoformans* AdSS, the loop located between residues 305-308 is turned towards IMP, presenting the IMP-binding residue R308 to the ligand. In the human structure, this loop is turned away from the empty IMP-binding site. This loop is also associated with the binding of l-aspartate and hadacidin, and is conserved between the two enzyme sequences. These structural changes are most likely to be the result of the presence of IMP in the cryptococal enzyme.

Both human and *C. neoformans* structures feature a complete and occupied GTP/GDP-binding site, allowing for a more comprehensive comparison. The areas adjacent to the GTP-binding site show significant structural changes, primarily the differing position of the aforementioned IMP/hadacidin/aspartate-binding loop, as well as the *C. neoformans*-specific B2 sheet extension. These differences result in an active site cleft that is more “open” above the bound GDP molecule in the *C. neoformans* structure (Fig 17A).

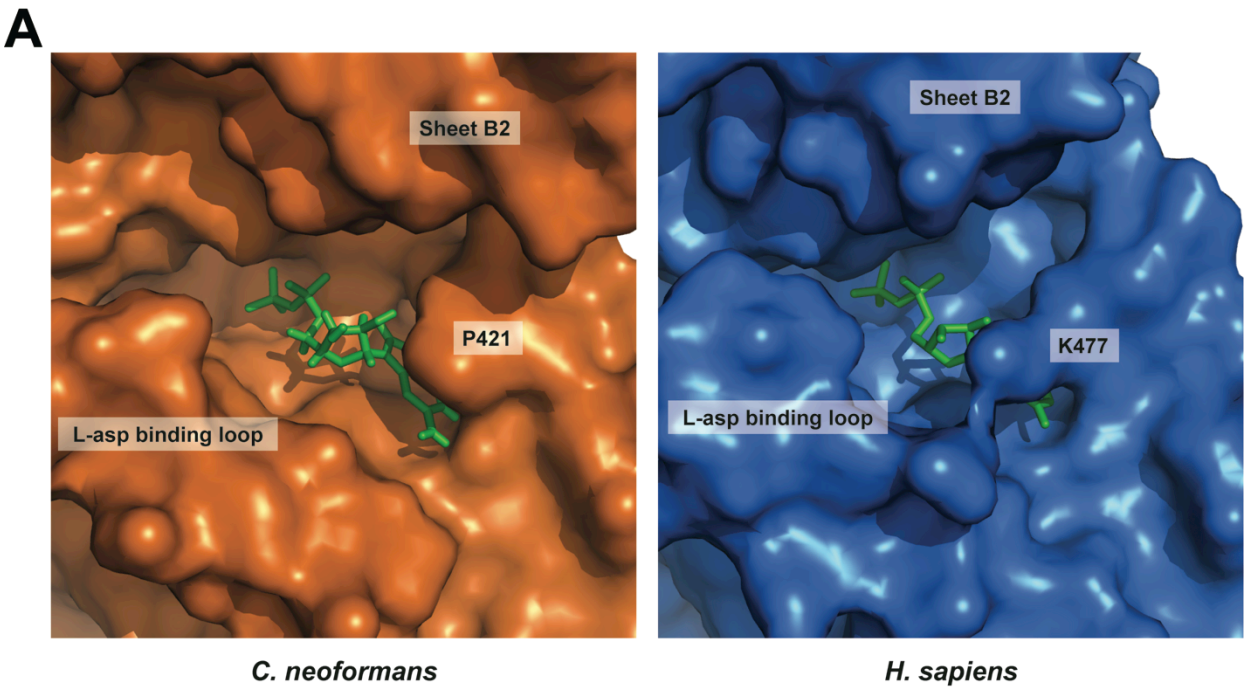

B

E. coli	406	LT.GVPIDIISTGPDRTETMILRDPFDA
S. cerevisiae	410	FV.GVPVEWVGTGPARESMLHKEIK...
A. fumigatus	402	ELGGVPIKWIGTGPARDHMICRE.....
C. neoformans	409	YL.GVKVQYVGVGPGRDQNVIIF.....
H. sapiens 1	436	HV.GVAVKWVGVGKSRESMIQLF.....
H. sapiens 2	435	EL.QIPVKWIGVGKSRESMIQLF.....
M. musculus 1	436	HM.GVAVKWVGVGKSRESMIQLF.....
M. musculus 2	435	EL.QIPVKWIGVGKSRESMIQLF.....

Fig 17. *Comparing the GDP binding site of fungal and human AdSS. (A) Comparison of the GTP-binding pockets from C. neoformans (orange, left) and H. sapiens (blue, right) AdSS. The structures are shown in surface representation. In H. sapiens AdSS, lysine 447 (B-factors: 23-32 Å2) projects across the active site, in contrast to proline 421 (B-factors: 68-72 Å2) in the equivalent position in C. neoformans AdSS. Also annotated are the B2 β-sheet, which is extended in C. neoformans, and the adjacent l-aspartate-binding loop. The PDB ID for the H. sapiens structure is 2V40. (B) Alignment of the C-terminal end of AdSS sequence from multiple species, with general conservation of residues annotated in black and variant lysine/proline residue annotated in green. Fungal and bacterial enzymes contain a proline at the marked position, while mammalian enzymes contain a lysine.*

The GDP-binding pocket itself is less variable between the two enzymes, but has one significant change. In humans, the side-chain of residue K447 projects across the GTP-binding crevice, close to the nucleobase end of the bound GDP. In *Cryptococcus*, this residue is replaced with a proline (P421) (Fig 17A). Interestingly, the alignment of AdSS sequences across several organisms shows that the *C. albicans*, *A. fumigatus*, *Arabidopsis thaliana* and *E. coli* enzymes also have a proline at this position. In comparison, both isoforms from humans and mice have a lysine at this position (Fig 17B).

Finally, the human enzyme also features a long segment at its N-terminus that does not appear in the sequence of the enzyme from *C. neoformans*, nor any of the lower eukaryotes or bacteria (Fig S1). This feature is present in both isoforms from both humans and mice, is 26 residues long in isoform 1 and 22 residues long in isoform 2, and is well conserved between species and isoforms. This region has not been modelled in the crystal structures from either mouse or human enzymes, suggesting it is flexible.

Chapter 7 – Discussion

With the increasing burden placed on our healthcare system by opportunistic fungal pathogens and the rise of antifungal resistance, new drug targets and novel antifungal compounds are urgently needed. Here, we have characterized the ubiquitous purine biosynthetic enzyme adenylosuccinate synthetase from the fungal pathogen *Cryptococcus neoformans.* In the process, we have revealed its potential as a target for the treatment of cryptococcal disease.

That the *C. neoformans ade12*Δ mutant displayed a loss of virulence, while the *aph1*Δ adenine salvage-deficient strain did not, is consistent with other studies into the importance of *de novo* purine metabolism in pathogenesis. Purine biosynthesis mutants of many bacterial pathogens, such as *Listeria monocytogenes* [(103)], *Yersinia pestis* [(104)], *Bacillus anthracis* [(105)] and *Staphylococcus aureus* [(106)], are avirulent. *C. albicans*, another opportunistic fungal pathogen, is also rendered avirulent by disruption of *de novo* purine biosynthesis [(107)].

The effects of disruption of purine salvage on microbial pathogens are not as well known. It has been known for over 40 years that obligate protozoan parasites are unable to synthesize purines *de novo* [(108)] and lack any of the required purine *de novo* biosynthetic genes [(109)]. Fittingly, purine salvage has been found to be essential in several obligate intracellular protozoan pathogens, including *Toxoplasma gondii* [(109)], *Plasmodium falciparum* [(110)] and *Leishmania donovani* [(111)], as well as the bacterial pathogen *Helicobacter pylori* [(112)]. While this would seem to run contrary to the ubiquity of the pathway in other organisms, the intracellular location of these parasites means that they can exploit their host's purine production, a luxury *C. neoformans* cannot enjoy due to its purine-poor niche in the central nervous system [(32)]. Indeed, our findings confirm that purine salvage via *Aph1* is not necessary or sufficient for *C. neoformans* during infection.

The dependence of *C. neoformans* on *de novo* purine biosynthesis during infection is in line with the model for *Cryptococcus* virulence suggested by our previous work with GTP biosynthetic enzymes [(31)]. In this model, purine salvage enzymes such as Aph1 and Hpt1 are dispensable for infection due to insufficient concentrations of environmental purines in the human central nervous system. During infection, *C. neoformans* must rely almost exclusively on *de novo* purine synthesis. Disruption of this pathway renders it avirulent

irrespective of virulence factor production, highlighting the potential of AdSS as an anticryptococcal drug target.

Hadacidin is an AdSS inhibitor that has been known to have antitumour activity since the early 1960s [(56)]. Despite being partially active against *C. neoformans* AdSS *in vitro*, hadacidin displayed no antifungal activity against *C. neoformans* cells, and only a limited degree of activity against *C. albicans*. This was possibly due to the concentrations of hadacidin tested *in vivo* being too low to engender an antifungal effect. However, even if hadacidin had been present in sufficient quantities to effect fungal growth, our *in vitro* assays suggests that it may not be able to fully inhibit the activity of *C. neoformans* AdSS on its own. The plateau in the inhibitory activity of hadacidin observed at high concentrations during our IC_{50} experiments indicates that not even therapeutically problematic millimolar concentrations of the drug would completely inhibit the enzyme. This is at odds with previous *in vitro* work completed using purified AdSS from *Dictyostelium discoideum* [(113)] and *E. coli* [(61)], which showed that 100% inhibition was possible at similar compound concentrations. *E. coli* enzyme studies performed by Tibrewal and Elliot [(61)] showed that the inhibitory activity of hadacidin decreased to 80% when the ratio of aspartate to hadacidin was increased from 1:1 to 5:1, suggesting a competitive inhibition of AdSS by hadacidin. Our assays using the *Crytococcus* AdSS were performed at a ratio higher than this, at least 10:1, due to the high concentration of aspartate required to saturate the *C. neoformans* enzyme. Indeed, the significantly higher K_M for aspartate exhibited by *C. neoformans* AdSS compared to *E. coli* indicates a difference in the two enzymes' affinity for aspartate, and therefore hadacidin or any other potential inhibitors targeting this binding pocket. This may explain the inability of hadacidin to completely inhibit the cryptococcal enzyme, and suggests that a full kinetic analysis of hadacidin and aspartate binding to AdSS would be useful. Since this would require us to synthesize large amounts of the inhibitor which is not currently commercially available, it is outside the scope of the current study.

AdSS has been crystallized in a variety of ligand-bound forms, with hadacidin acting as a common stand-in for l-aspartate during attempts to crystallize a fully ligated enzyme. Previous studies with the *E. coli* and mouse enzymes have reported that, when crystallized with IMP and GTP, AdSS was resolved as a stable complex with GDP and the intermediate 6-PIMP regardless of the inclusion or absence of hadacidin [(98, 114)]. This corresponds to a “frozen” intermediate state in the AdSS reaction, in which the γ-phosphate of GTP is transferred to the 6-oxygen position of IMP. The reaction is unable to

continue to completion without l-aspartate. In our structure, there is no visible electron density supporting the presence of a phosphate group at the γ position of GDP, indicating that the initial hydrolysis of GTP has taken place in the crystallized complex. However, no corresponding phosphate was detected at the 6-oxygen position of IMP. This may indicate that the AdSS-IMP-GTP/GDP complex was captured here in a state of flux between the two binding states, that GTP was hydrolyzed to GDP before crystal formation began and bound to the GTP binding pocket regardless (a complex seen in other GDP-bound AdSS structures, including the human structure used in this study), or that it was hydrolyzed in the time it took for crystals to form.

Despite this, we were still able to use our ligated crystal structure to directly compare the GDP-binding sites of *C. neoformans* and human AdSS in their bound contexts, a significant step forward in the process of designing species-specific AdSS inhibitors. The GDP-binding site is well resolved in *C. neoformans* and human AdSS structures and exhibits one of the most significant observable difference between the two enzymes – the replacement of a lysine side-chain in the human enzyme with a proline in the *C. neoformans* enzyme. These amino acids have markedly different properties; lysine side-chains are flexible and are often involved in hydrogen bonding, and carry a positive charge, while proline side-chains are rigid and uncharged. In the human structure, this lysine projects across the GTP-binding site, while the much shorter proline does not.

This divergence in the GTP-binding site may help explain the differences in GTP K_M values between the cryptococcal and mammalian enzymes (Table 1), although further investigation into both the human and *C. neoformans* crystal structures and kinetic mechanisms would be required to confirm this. Additionally, the fact that that the bacterial, fungal and plant orthologs of AdSS share a proline at this residue, while human and mouse sequences share a lysine, suggest that this lysine may be a mammalian-specific feature. If this is true, it may be possible to use this change in residues to design inhibitors with a broad spectrum of antimicrobial activity that still maintain the specificity needed to avoid harming mammalian patients.

The second significant difference between the human and *C. neoformans* structure is the *Cryptococcus*-specific extension to the B2 β-sheet. While this feature is located adjacent to the GDP-binding site, and was only fully resolved in the ligand-bound protein structure, it does not appear to be directly involved in substrate binding. The function, if any, of this extended sheet could be further determined via targeted deletion mutation experiments.

The mismatched resolution of this segment between the two chains of our crystal structure is most likely related to the packing of molecules in our crystals.

In summary, here I have demonstrated that ATP biosynthesis is crucial for *C. neoformans* virulence, but not for virulence factor production. In contrast, adenine salvage is neither necessary nor sufficient for cryptococcal virulence. I have characterised the kinetic parameters of the purine biosynthetic enzyme AdSS, and tested the efficacy of an existing AdSS inhibitor on the fungal enzyme, as well as living cells. I have also presented the first crystal structure of an AdSS enzyme from a fungal species, and described the species-specific differences in the otherwise-conserved AdSS that mark it as a strong candidate for further development of inhibitors. In particular, the discovery of a proline residue in the enzyme's GTP-binding pocket that is conserved in fungal, bacterial and plant species, but not in mammals, paves the way for the potential development of agents with a broad-spectrum of antimicrobial and herbicidal activity.

References

1. UNAIDS. (2012) 2012 UNAIDS Report on the Global AIDS Epidemic, Joint United Nations Programme on HIV/AIDS (UNAIDS).
2. Fishman, J. A. (2007) Infection in solid-organ transplant recipients, *The New England journal of medicine 357*, 2601-2614.
3. Rojas, Y., Finnerty, C. C., Radhakrishnan, R. S., and Herndon, D. N. (2012) Burns: an update on current pharmacotherapy, *Expert opinion on pharmacotherapy 13*, 2485-2494.
4. Hoffman, G. S. (1993) Immunosuppressive therapy for autoimmune diseases, *Annals of allergy 70*, 263-274.
5. Parvaneh, N., Casanova, J. L., Notarangelo, L. D., and Conley, M. E. (2013) Primary immunodeficiencies: a rapidly evolving story, *The Journal of allergy and clinical immunology 131*, 314-323.
6. Ting, C., Bansal, V., Batal, I., Mounayar, M., Chabtini, L., El Akiki, G., and Azzi, J. (2012) Impairment of immune systems in diabetes, *Advances in experimental medicine and biology 771*, 62-75.
7. Bodey, G. P. (1986) Infection in cancer patients. A continuing association, *The American journal of medicine 81*, 11-26.
8. Park, B. J., Wannemuehler, K. A., Marston, B. J., Govender, N., Pappas, P. G., and Chiller, T. M. (2009) Estimation of the current global burden of cryptococcal meningitis among persons living with HIV/AIDS, *Aids 23*, 525-530.
9. Sukroongreung, S., Kitiniyom, K., Nilakul, C., and Tantimavanich, S. (1998) Pathogenicity of basidiospores of Filobasidiella neoformans var. neoformans, *Medical mycology : official publication of the International Society for Human and Animal Mycology 36*, 419-424.
10. Alspaugh, J. A., Cavallo, L. M., Perfect, J. R., and Heitman, J. (2000) RAS1 regulates filamentation, mating and growth at high temperature of Cryptococcus neoformans, *Molecular microbiology 36*, 352-365.
11. Bose, I., Reese, A. J., Ory, J. J., Janbon, G., and Doering, T. L. (2003) A yeast under cover: the capsule of Cryptococcus neoformans, *Eukaryotic cell 2*, 655-663.
12. McFadden, D. C., and Casadevall, A. (2001) Capsule and melanin synthesis in Cryptococcus neoformans, *Medical mycology : official publication of the International Society for Human and Animal Mycology 39 Suppl 1*, 19-30.
13. Nosanchuk, J. D., Rudolph, J., Rosas, A. L., and Casadevall, A. (1999) Evidence that Cryptococcus neoformans is melanized in pigeon excreta: implications for pathogenesis, *Infection and immunity 67*, 5477-5479.
14. Zhu, X., and Williamson, P. R. (2004) Role of laccase in the biology and virulence of Cryptococcus neoformans, *FEMS yeast research 5*, 1-10.
15. Casadevall, A., Rosas, A. L., and Nosanchuk, J. D. (2000) Melanin and virulence in Cryptococcus neoformans, *Current opinion in microbiology 3*, 354-358.
16. Odds, F. C., Brown, A. J., and Gow, N. A. (2003) Antifungal agents: mechanisms of action, *Trends in microbiology 11*, 272-279.
17. Vanden Bossche, H., Koymans, L., and Moereels, H. (1995) P450 inhibitors of use in medical treatment: focus on mechanisms of action, *Pharmacology & therapeutics 67*, 79-100.
18. Yoshida, Y. (1988) Cytochrome P450 of fungi: primary target for azole antifungal agents, *Current topics in medical mycology 2*, 388-418.
19. Ostrosky-Zeichner, L., Casadevall, A., Galgiani, J. N., Odds, F. C., and Rex, J. H. (2010) An insight into the antifungal pipeline: selected new molecules and beyond, *Nat Rev Drug Discov 9*, 719-727.
20. Gruszecki, W. I., Gagos, M., Herec, M., and Kernen, P. (2003) Organization of antibiotic amphotericin B in model lipid membranes. A mini review, *Cellular & molecular biology letters 8*, 161-170.
21. Kotler-Brajtburg, J., Price, H. D., Medoff, G., Schlessinger, D., and Kobayashi, G. S. (1974) Molecular basis for the selective toxicity of amphotericin B for yeast and filipin for animal cells, *Antimicrob Agents Chemother 5*, 377-382.

22. Readio, J. D., and Bittman, R. (1982) Equilibrium binding of amphotericin B and its methyl ester and borate complex to sterols, *Biochimica et biophysica acta 685*, 219-224.
23. Hamill, R. J. (2013) Amphotericin B formulations: a comparative review of efficacy and toxicity, *Drugs 73*, 919-934.
24. Ostrosky-Zeichner, L., Marr, K. A., Rex, J. H., and Cohen, S. H. (2003) Amphotericin B: time for a new "gold standard", *Clinical infectious diseases : an official publication of the Infectious Diseases Society of America 37*, 415-425.
25. Hauser, D., and Sigg, H. P. (1971) [Isolation and decomposition of sordarin], *Helvetica chimica acta 54*, 1178-1190.
26. Liang, H. (2008) Sordarin, an antifungal agent with a unique mode of action, *Beilstein journal of organic chemistry 4*, 31.
27. Dominguez, J. M., and Martin, J. J. (1998) Identification of elongation factor 2 as the essential protein targeted by sordarins in Candida albicans, *Antimicrob. Agents Chemother. 42*, 2279-2283.
28. Elion, G. B. (1989) The purine path to chemotherapy, *Science 244*, 41-47.
29. Franklin, T. J., and Cook, J. M. (1969) The inhibition of nucleic acid synthesis by mycophenolic acid, *The Biochemical journal 113*, 515-524.
30. Clarke, D. A., Philips, F. S., Sternberg, S. S., Stock, C. C., Elion, G. B., and Hitchings, G. H. (1953) 6-Mercaptopurine: effects in mouse sarcoma 180 and in normal animals, *Cancer research 13*, 593-604.
31. Morrow, C. A., Valkov, E., Stamp, A., Chow, E. W., Lee, I. R., Wronski, A., Williams, S. J., Hill, J. M., Djordjevic, J. T., Kappler, U., Kobe, B., and Fraser, J. A. (2012) De novo GTP Biosynthesis Is Critical for Virulence of the Fungal Pathogen Cryptococcus neoformans, *PLoS pathogens 8*, e1002957.
32. Eells, J. T., and Spector, R. (1983) Purine and pyrimidine base and nucleoside concentrations in human cerebrospinal fluid and plasma, *Neurochemical research 8*, 1451-1457.
33. Morrow, C. A., Stamp, A., Valkov, E., Kobe, B., and Fraser, J. A. (2010) Crystallization and preliminary X-ray analysis of mycophenolic acid-resistant and mycophenolic acid-sensitive forms of IMP dehydrogenase from the human fungal pathogen Cryptococcus, *Acta crystallographica. Section F, Structural biology and crystallization communications 66*, 1104-1107.
34. Lowy, B., and Dorfman, B. Z. (1970) Adenylosuccinase activity in human and rabbit erythrocyte lysates, *The Journal of biological chemistry 245*, 3043-3046.
35. Hassan, H. F., and Coombs, G. H. (1988) Purine and pyrimidine metabolism in parasitic protozoa, *FEMS microbiology reviews 4*, 47-83.
36. Lowenstein, J. M. (1990) The purine nucleotide cycle revisited [corrected], *International journal of sports medicine 11 Suppl 2*, S37-46.
37. Matsuda, Y., Ogawa, H., Fukutome, S., Shiraki, H., and Nakagawa, H. (1977) Adenylosuccinate synthetase in rat liver: the existence of two types and their regulatory roles, *Biochemical and biophysical research communications 78*, 766-771.
38. Van den Berghe, G., Bontemps, F., Vincent, M. F., and Van den Bergh, F. (1992) The purine nucleotide cycle and its molecular defects, *Progress in neurobiology 39*, 547-561.
39. Lieberman, I. (1956) Enzymatic synthesis of adenosine-5'-phosphate from inosine-5'-phosphate, *The Journal of biological chemistry 223*, 327-339.
40. Poland, B. W., Silva, M. M., Serra, M. A., Cho, Y., Kim, K. H., Harris, E. M., and Honzatko, R. B. (1993) Crystal structure of adenylosuccinate synthetase from Escherichia coli. Evidence for convergent evolution of GTP-binding domains, *The Journal of biological chemistry 268*, 25334-25342.
41. Silva, M. M., Poland, B. W., Hoffman, C. R., Fromm, H. J., and Honzatko, R. B. (1995) Refined crystal structures of unligated adenylosuccinate synthetase from Escherichia coli, *J Mol Biol 254*, 431-446.
42. Liu, F., Dong, Q., and Fromm, H. J. (1992) Site-directed mutagenesis of the phosphate-binding consensus sequence in Escherichia coli adenylosuccinate synthetase, *The Journal of biological chemistry 267*, 2388-2392.

43. Kang, C., and Fromm, H. J. (1994) Characterization of the putative GTP-binding site residues of Escherichia coli adenylosuccinate synthetase by site-directed mutagenesis, *Arch Biochem Biophys 310*, 475-480.
44. Hou, Z., Wang, W., Fromm, H. J., and Honzatko, R. B. (2002) IMP Alone Organizes the Active Site of Adenylosuccinate Synthetase from Escherichia coli, *The Journal of biological chemistry 277*, 5970-5976.
45. Wang, W., Gorrell, A., Honzatko, R. B., and Fromm, H. J. (1997) A study of Escherichia coli adenylosuccinate synthetase association states and the interface residues of the homodimer, *The Journal of biological chemistry 272*, 7078-7084.
46. Kang, C., Kim, S., and Fromm, H. J. (1996) Subunit complementation of Escherichia coli adenylosuccinate synthetase, *The Journal of biological chemistry 271*, 29722-29728.
47. Moe, O. A., Baker-Malcolm, J. F., Wang, W., Kang, C., Fromm, H. J., and Colman, R. F. (1996) Involvement of arginine 143 in nucleotide substrate binding at the active site of adenylosuccinate synthetase from Escherichia coli, *Biochemistry 35*, 9024-9033.
48. Eaazhisai, K., Jayalakshmi, R., Gayathri, P., Anand, R. P., Sumathy, K., Balaram, H., and Murthy, M. R. (2004) Crystal structure of fully ligated adenylosuccinate synthetase from Plasmodium falciparum, *J Mol Biol 335*, 1251-1264.
49. Prade, L., Cowan-Jacob, S. W., Chemla, P., Potter, S., Ward, E., and Fonne-Pfister, R. (2000) Structures of adenylosuccinate synthetase from Triticum aestivum and Arabidopsis thaliana, *J Mol Biol 296*, 569-577.
50. Iancu, C. V., Borza, T., Choe, J. Y., Fromm, H. J., and Honzatko, R. B. (2001) Recombinant mouse muscle adenylosuccinate synthetase: overexpression, kinetics, and crystal structure, *The Journal of biological chemistry 276*, 42146-42152.
51. Murthy, Y. K., Thiemann, J. E., Coronelli, C., and Sensi, P. (1966) Alanosine, a new antiviral and antitumour agent isolated from a Streptomyces, *Nature 211*, 1198-1199.
52. Graff, J. C., and Plagemann, P. G. (1976) Alanosine toxicity in Novikoff rat hepatoma cells due to inhibition of the conversion of inosine monophosphate to adenosine monophosphate, *Cancer research 36*, 1428-1440.
53. Gale, G. R., and Smith, A. B. (1968) Alanosine and hadacidin--comparison of effects on adenylosuccinate synthetase, *Biochemical pharmacology 17*, 2495-2498.
54. Tyagi, A. K., and Cooney, D. A. (1980) Identification of the antimetabolite of L-alanosine, L-alanosyl-5-amino-4-imidazolecarboxylic acid ribonucleotide, in tumors and assessment of its inhibition of adenylosuccinate synthetase, *Cancer research 40*, 4390-4397.
55. Kindler, H. L., Burris, H. A., 3rd, Sandler, A. B., and Oliff, I. A. (2009) A phase II multicenter study of L-alanosine, a potent inhibitor of adenine biosynthesis, in patients with MTAP-deficient cancer, *Investigational new drugs 27*, 75-81.
56. Kaczka, E. A., Gitterman, C. O., Dulaney, E. L., and Folkers, K. (1962) Hadacidin, a new growth-inhibitory substance in human tumor systems, *Biochemistry 1*, 340-343.
57. Gray, R. A., Gauger, G. W., Dulaney, E. L., Kaczka, E. A., and Woodruff, H. B. (1964) Hadacidin, a New Plant-Growth Inhibitor Produced by Fermentation, *Plant physiology 39*, 204-207.
58. Demain, A. L. (1966) Mode of action of hadacidin in the growing bacterial cell, *Nature 212*, 93-94.
59. Shigeura, H. T., and Gordon, C. N. (1962) The mechanism of action of hadacidin, *The Journal of biological chemistry 237*, 1937-1940.
60. Shigeura, H. T., and Gordon, C. N. (1962) Hadacidin, a new inhibitor of purine biosynthesis, *The Journal of biological chemistry 237*, 1932-1936.
61. Tibrewal, N., and Elliott, G. I. (2011) Evaluation of hadacidin analogues, *Bioorganic & medicinal chemistry letters 21*, 517-519.
62. Nakajima, M., Itoi, K., Takamatsu, Y., Kinoshita, T., Okazaki, T., Kawakubo, K., Shindo, M., Honma, T., Tohjigamori, M., and Haneishi, T. (1991) Hydantocidin: a new compound with herbicidal activity from Streptomyces hygroscopicus, *The Journal of antibiotics 44*, 293-300.
63. Fonne-Pfister, R., Chemla, P., Ward, E., Girardet, M., Kreuz, K. E., Honzatko, R. B., Fromm, H. J., Schar, H. P., Grutter, M. G., and Cowan-Jacob, S. W. (1996) The mode of action and the structure of a herbicide in complex with its target: binding of activated hydantocidin to the feedback regulation site of adenylosuccinate synthetase, *Proceedings of the National Academy of Sciences of the United States of America 93*, 9431-9436.

64. Hanessian, S., Lu, P. P., Sanceau, J. Y., Chemla, P., Gohda, K., Fonne-Pfister, R., Prade, L., and Cowan-Jacob, S. W. (1999) An Enzyme-Bound Bisubstrate Hybrid Inhibitor of Adenylosuccinate Synthetase, *Angew Chem Int Ed Engl 38*, 3159-3162.
65. Janbon, G., Ormerod, K. L., Paulet, D., Byrnes, E. J., 3rd, Yadav, V., Chatterjee, G., Mullapudi, N., Hon, C. C., Billmyre, R. B., Brunel, F., Bahn, Y. S., Chen, W., Chen, Y., Chow, E. W., Coppee, J. Y., Floyd-Averette, A., Gaillardin, C., Gerik, K. J., Goldberg, J., Gonzalez-Hilarion, S., Gujja, S., Hamlin, J. L., Hsueh, Y. P., Ianiri, G., Jones, S., Kodira, C. D., Kozubowski, L., Lam, W., Marra, M., Mesner, L. D., Mieczkowski, P. A., Moyrand, F., Nielsen, K., Proux, C., Rossignol, T., Schein, J. E., Sun, S., Wollschlaeger, C., Wood, I. A., Zeng, Q., Neuveglise, C., Newlon, C. S., Perfect, J. R., Lodge, J. K., Idnurm, A., Stajich, J. E., Kronstad, J. W., Sanyal, K., Heitman, J., Fraser, J. A., Cuomo, C. A., and Dietrich, F. S. (2014) Analysis of the genome and transcriptome of Cryptococcus neoformans var. grubii reveals complex RNA expression and microevolution leading to virulence attenuation, *PLoS genetics 10*, e1004261.
66. Fraser, J. A., Subaran, R. L., Nichols, C. B., and Heitman, J. (2003) Recapitulation of the sexual cycle of the primary fungal pathogen Cryptococcus neoformans var. gattii: implications for an outbreak on Vancouver Island, Canada, *Eukaryotic cell 2*, 1036-1045.
67. Idnurm, A., Reedy, J. L., Nussbaum, J. C., and Heitman, J. (2004) Cryptococcus neoformans virulence gene discovery through insertional mutagenesis, *Eukaryotic cell 3*, 420-429.
68. Arras, S. D., Chitty, J. L., Blake, K. L., Schulz, B. L., and Fraser, J. A. (2015) A genomic safe haven for mutant complementation in Cryptococcus neoformans, *PLoS One 10*, e0122916.
69. Sambrook, J., Maniatis, T., and Fritsch, E. F. (1989) *Molecular cloning: a laboratory manual*, Vol. 2nd, Cold Spring Harbor Laboratory, Cold Spring Harbor, N.Y - Book.
70. Pitkin, J. W., Panaccione, D. G., and Walton, J. D. (1996) A putative cyclic peptide efflux pump encoded by the TOXA gene of the plant-pathogenic fungus Cochliobolus carbonum, *Microbiology 142 (Pt 6)*, 1557-1565.
71. Davidson, R. C., Cruz, M. C., Sia, R. A., Allen, B., Alspaugh, J. A., and Heitman, J. (2000) Gene disruption by biolistic transformation in serotype D strains of Cryptococcus neoformans, *Fungal genetics and biology : FG & B 29*, 38-48.
72. Toffaletti, D. L., Rude, T. H., Johnston, S. A., Durack, D. T., and Perfect, J. R. (1993) Gene-transfer in Cryptococcus-neoformans by use of biolistic delivery of DNA, *Journal of bacteriology 175*, 1405-1411.
73. Fraser, J. A., Subaran, R. L., Nichols, C. B., and Heitman, J. (2003) Recapitulation of the sexual cycle of the primary fungal pathogen Cryptococcus neoformans var. gattii: Implications for an outbreak on Vancouver Island, Canada, *Eukaryotic cell 2*, 1036-1045.
74. McDade, H. C., and Cox, G. M. (2001) A new dominant selectable marker for use in Cryptococcus neoformans, *Medical mycology : official publication of the International Society for Human and Animal Mycology 39*, 151-154.
75. D'Souza, C. A., Alspaugh, J. A., Yue, C., Harashima, T., Cox, G. M., Perfect, J. R., and Heitman, J. (2001) Cyclic AMP-dependent protein kinase controls virulence of the fungal pathogen Cryptococcus neoformans, *Molecular and cellular biology 21*, 3179-3191.
76. Chen, S. C. A., Muller, M., Zhou, J. Z., Wright, L. C., and Sorrell, T. C. (1997) Phospholipase activity in Cryptococcus neoformans: A new virulence factor?, *J Infect Dis 175*, 414-420.
77. (2005) Reference method for broth dilution antifungal susceptibility testing of yeasts; approved standard-second edition. CLSI document M27-A2, Clinical and Laboratory Standards Institute., Wayne, PA.
78. Morrow, C. A., Lee, I. R., Chow, E. W., Ormerod, K. L., Goldinger, A., Byrnes, E. J., 3rd, Nielsen, K., Heitman, J., Schirra, H. J., and Fraser, J. A. (2012) A unique chromosomal rearrangement in the Cryptococcus neoformans var. grubii type strain enhances key phenotypes associated with virulence, *mBio 3*.
79. Cox, G. M., Mukherjee, J., Cole, G. T., Casadevall, A., and Perfect, J. R. (2000) Urease as a virulence factor in experimental cryptococcosis, *Infection and immunity 68*, 443-448.
80. Blundell, R. D., Williams, S. J., Morrow, C. A., Ericsson, D. J., Kobe, B., and Fraser, J. A. (2013) Purification, crystallization and preliminary X-ray analysis of adenylosuccinate

synthetase from the fungal pathogen Cryptococcus neoformans, *Acta Crystallographica Section F 69*, 1033-1036.
81. Kabsch, W. (2010) Xds, *Acta crystallographica. Section D, Biological crystallography 66*, 125-132.
82. Winn, M. D., Ballard, C. C., Cowtan, K. D., Dodson, E. J., Emsley, P., Evans, P. R., Keegan, R. M., Krissinel, E. B., Leslie, A. G., McCoy, A., McNicholas, S. J., Murshudov, G. N., Pannu, N. S., Potterton, E. A., Powell, H. R., Read, R. J., Vagin, A., and Wilson, K. S. (2011) Overview of the CCP4 suite and current developments, *Acta crystallographica. Section D, Biological crystallography 67*, 235-242.
83. McCoy, A. J., Grosse-Kunstleve, R. W., Adams, P. D., Winn, M. D., Storoni, L. C., and Read, R. J. (2007) Phaser crystallographic software, *Journal of applied crystallography 40*, 658-674.
84. Terwilliger, T. C., Grosse-Kunstleve, R. W., Afonine, P. V., Moriarty, N. W., Zwart, P. H., Hung, L. W., Read, R. J., and Adams, P. D. (2008) Iterative model building, structure refinement and density modification with the PHENIX AutoBuild wizard, *Acta crystallographica. Section D, Biological crystallography 64*, 61-69.
85. Adams, P. D., Afonine, P. V., Bunkoczi, G., Chen, V. B., Davis, I. W., Echols, N., Headd, J. J., Hung, L. W., Kapral, G. J., Grosse-Kunstleve, R. W., McCoy, A. J., Moriarty, N. W., Oeffner, R., Read, R. J., Richardson, D. C., Richardson, J. S., Terwilliger, T. C., and Zwart, P. H. (2010) PHENIX: a comprehensive Python-based system for macromolecular structure solution, *Acta crystallographica. Section D, Biological crystallography 66*, 213-221.
86. Afonine, P. V., Grosse-Kunstleve, R. W., Echols, N., Headd, J. J., Moriarty, N. W., Mustyakimov, M., Terwilliger, T. C., Urzhumtsev, A., Zwart, P. H., and Adams, P. D. (2012) Towards automated crystallographic structure refinement with phenix.refine, *Acta crystallographica. Section D, Biological crystallography 68*, 352-367.
87. Emsley, P., Lohkamp, B., Scott, W. G., and Cowtan, K. (2010) Features and development of Coot, *Acta crystallographica. Section D, Biological crystallography 66*, 486-501.
88. Lipps, G., and Krauss, G. (1999) Adenylosuccinate synthase from Saccharomyces cerevisiae: homologous overexpression, purification and characterization of the recombinant protein, *The Biochemical journal 341 (Pt 3)*, 537-543.
89. Fromm, H. J. (1958) On the equilibrium and mechanism of adenylosuccinic acid synthesis, *Biochimica et biophysica acta 29*, 255-262.
90. Jayalakshmi, R., Sumathy, K., and Balaram, H. (2002) Purification and characterization of recombinant Plasmodium falciparum adenylosuccinate synthetase expressed in Escherichia coli, *Protein Expr Purif 25*, 65-72.
91. Sun, H., Li, N., Wang, X., Chen, T., Shi, L., Zhang, L., Wang, J., Wan, T., and Cao, X. (2005) Molecular cloning and characterization of a novel muscle adenylosuccinate synthetase, AdSSL1, from human bone marrow stromal cells, *Molecular and cellular biochemistry 269*, 85-94.
92. Idnurm, A., Bahn, Y. S., Nielsen, K., Lin, X. R., Fraser, J. A., and Heitman, J. (2005) Deciphering the model pathogenic fungus Cryptococcus neoformans, *Nat. Rev. Microbiol. 3*, 753-764.
93. Emri, T., Majoros, L., Toth, V., and Pocsi, I. (2013) Echinocandins: production and applications, *Applied microbiology and biotechnology*.
94. Wang, W., Poland, B. W., Honzatko, R. B., and Fromm, H. J. (1995) Identification of arginine residues in the putative L-aspartate binding site of Escherichia coli adenylosuccinate synthetase, *The Journal of biological chemistry 270*, 13160-13163.
95. Honzatko, R. B., and Fromm, H. J. (1999) Structure-function studies of adenylosuccinate synthetase from Escherichia coli, *Arch Biochem Biophys 370*, 1-8.
96. Alfonzo, J. D., Sahota, A., and Taylor, M. W. (1997) Purification and characterization of adenine phosphoribosyltransferase from Saccharomyces cerevisiae, *Biochimica et biophysica acta 1341*, 173-182.
97. Poland, B. W., Hou, Z., Bruns, C., Fromm, H. J., and Honzatko, R. B. (1996) Refined crystal structures of guanine nucleotide complexes of adenylosuccinate synthetase from Escherichia coli, *The Journal of biological chemistry 271*, 15407-15413.

98. Choe, J. Y., Poland, B. W., Fromm, H. J., and Honzatko, R. B. (1999) Mechanistic implications from crystalline complexes of wild-type and mutant adenylosuccinate synthetases from Escherichia coli, *Biochemistry 38*, 6953-6961.
99. Iancu, C. V., Borza, T., Fromm, H. J., and Honzatko, R. B. (2002) Feedback inhibition and product complexes of recombinant mouse muscle adenylosuccinate synthetase, *The Journal of biological chemistry 277*, 40536-40543.
100. Wang, X., Akasaka, R., Takemoto, C., Morita, S., Yamaguchi, M., Terada, T., Shirozu, M., Yokoyama, S., Chen, S., Si, S., and Xie, Y. (2011) Overexpression, purification, crystallization and preliminary crystallographic studies of a hyperthermophilic adenylosuccinate synthetase from Pyrococcus horikoshii OT3, *Acta crystallographica. Section F, Structural biology and crystallization communications 67*, 1551-1555.
101. Kabsch, W. (2010) Integration, scaling, space-group assignment and post-refinement, *Acta crystallographica. Section D, Biological crystallography 66*, 133-144.
102. Matthews, B. W. (1968) Solvent content of protein crystals, *J Mol Biol 33*, 491-497.
103. Faith, N. G., Kim, J. W., Azizoglu, R., Kathariou, S., and Czuprynski, C. (2012) Purine biosynthesis mutants (purA and purB) of serotype 4b Listeria monocytogenes are severely attenuated for systemic infection in intragastrically inoculated A/J Mice, *Foodborne pathogens and disease 9*, 480-486.
104. Brubaker, R. R. (1970) Interconversion of Purine Mononucleotides in Pasteurella pestis, *Infection and immunity 1*, 446-454.
105. Ivanovics, G., Marjai, E., and Dobozy, A. (1968) The growth of purine mutants of Bacillus anthracis in the body of the mouse, *Journal of general microbiology 53*, 147-162.
106. Lan, L., Cheng, A., Dunman, P. M., Missiakas, D., and He, C. (2010) Golden pigment production and virulence gene expression are affected by metabolisms in Staphylococcus aureus, *Journal of bacteriology 192*, 3068-3077.
107. Jiang, L., Zhao, J., Guo, R., Li, J., Yu, L., and Xu, D. (2010) Functional characterization and virulence study of ADE8 and GUA1 genes involved in the de novo purine biosynthesis in Candida albicans, *FEMS yeast research 10*, 199-208.
108. Booden, T., and Hull, R. W. (1973) Nucleic acid precursor synthesis by Plasmodium lophurae parasitizing chicken erythrocytes, *Experimental parasitology 34*, 220-228.
109. Chaudhary, K., Darling, J. A., Fohl, L. M., Sullivan, W. J., Jr., Donald, R. G., Pfefferkorn, E. R., Ullman, B., and Roos, D. S. (2004) Purine salvage pathways in the apicomplexan parasite Toxoplasma gondii, *The Journal of biological chemistry 279*, 31221-31227.
110. Downie, M. J., Kirk, K., and Mamoun, C. B. (2008) Purine salvage pathways in the intraerythrocytic malaria parasite Plasmodium falciparum, *Eukaryotic cell 7*, 1231-1237.
111. Boitz, J. M., Strasser, R., Hartman, C. U., Jardim, A., and Ullman, B. (2012) Adenine aminohydrolase from Leishmania donovani: unique enzyme in parasite purine metabolism, *The Journal of biological chemistry 287*, 7626-7639.
112. Liechti, G., and Goldberg, J. B. (2012) Helicobacter pylori relies primarily on the purine salvage pathway for purine nucleotide biosynthesis, *Journal of bacteriology 194*, 839-854.
113. Jahngen, E. G., and Rossomando, E. F. (1984) Adenylosuccinate synthetase from Dictyostelium discoideum: effects of hadacidin analogs and binding of [14C]hadacidin, *Arch Biochem Biophys 229*, 145-154.
114. Iancu, C. V., Borza, T., Fromm, H. J., and Honzatko, R. B. (2002) IMP, GTP, and 6-phosphoryl-IMP complexes of recombinant mouse muscle adenylosuccinate synthetase, *The Journal of biological chemistry 277*, 26779-26787.

Appendices

Table S1: Primers used in this project

Name	Purpose	Sequence
UQ1742	*ADE12* 5' flank overlap forward	AGCTTGAAATAACACACACGC
UQ1743	*ADE12* 5' flank overlap reverse	TCCAGCTCACATCCTCGCAGCCTAGAATAGATAGG
UQ1744	*ADE12* 3' flank overlap forward	CCGTGTTAATACAGATAAACCGAAGATCGAAAGTT
UQ1745	*ADE12* 3' flank overlap reverse	TTTCATTACGTACCCAGAACC
UQ1830	*ADE12 NEO* overlap forward	CCTATCTATTCTAGGCTGCGAGGATGTGAGCTGGAG
UQ1831	*ADE12 NEO* overlap reverse	AAACTTTCGATCTTCGGTTTATCTGTATTAACACGG
UQ1750	*APH1* 5' flank overlap forward	AGATGACTAACCGGGAGGTAA
UQ1751	*APH1* 5' flank overlap reverse	CAGCTCACATCCTCGCAGCGGTGGAAAGGGTGTGT
UQ1752	*APH1* 3' flank overlap forward	GTTAATACAGATAAACCAGGTCAAGGGTATTTTAG
UQ1753	*APH1* 3' flank overlap reverse	AAGTGTCCTGTCCAAGCCAGA
UQ1834	*APH1 NEO* overlap forward	ACACACCCTTTCCACCGCTGCGAGGATGTGAGCTGG
UQ1835	*APH1 NEO* overlap reverse	ACTAAAATACCCTTGACCTGGTTTATCTGTATTAAC
UQ2051	*ADE12* TOPO sequencing primer 1	GGCATTTATTAATCATTCTCA
UQ2052	*ADE12* TOPO sequencing primer 2	ACGTCCCTTCGCTTTTCAATG
UQ2053	*ADE12* TOPO sequencing primer 3	GTGTCGTCGGTGTCATCAAGG
UQ2054	*ADE12* TOPO sequencing primer 4	AAGGTTCAATACGTCGGTGTT
UQ2055	*ADE12* TOPO sequencing primer 5	TGTTGTGTTGTGTTCGCTGTG
UQ2063	*APH1* TOPO sequencing primer 1	TTACGGGCTTCACGCTTTTCG

UQ2064	*APH1* TOPO sequencing primer 2	ACACACAGGGCATCACCTTCC
UQ2065	*APH1* TOPO sequencing primer 3	CCCGTTTACTCCATGATTGAG
UQ2066	*APH1* TOPO sequencing primer 4	GGGGGCTGAAAACCATAGTAT
UQ2259	*ADE12* expression upper	ACGCACGGATCCATGGCTCCATCCCCGGAGGGA
UQ2260	*ADE12 expression lower*	GAACGTCTGCAGTTAGAAGATGATAACGTTCTG

Table S2: Fungal strains used in this project.

Strain	Species	Strain Details	Source
H99	*Cryptococcus neoformans* var. *grubii*	Laboratory type-strain	John Perfect
SDMA17	*Cryptococcus neoformans* var. *grubii*	*ade12::NEO*	This study
RBD01	*Cryptococcus neoformans* var. *grubii*	*ade12::NEO ADE12-NAT*	This study
AK3	*Cryptococcus neoformans* var. *grubii*	*aph1::NEO*	This study
KLB02	*Cryptococcus neoformans* var. *grubii*	*aph1::NEO APH1-NAT*	This study
ATCC 90113	*Cryptococcus neoformans* var. *grubii*	ATCC reference strain	ATCC
ATCC 90028	*Candida albicans*	ATCC reference strain	ATCC
ATCC 90030	*Candida galbrata*	ATCC reference strain	ATCC
ATCC 22019	*Candida parapsilosis*	ATCC reference strain	ATCC
ATCC MYA-3626	*Aspergillus fumigatus*	ATCC reference strain	ATCC

Table S3: Crystallographic statistics for *C. neoformans* AdSS structures. Statistics for the highest-resolution shell are shown in parentheses. All statistics generated by Phenix.

Diffraction data statistics	***Apo AdSS***	***Ligated AdSS***
Space group	*P 2₁ 2₁ 2₁*	*P 2₁ 2₁ 2₁*
Unit cell parameters a, b, c (Å); α=β=γ (°)	58.08, 101.00, 163.80; 90	55.81, 100.77, 163.80; 90
Molecules per asymmetric unit	2	2
Resolution range (Å)	37.02 - 2.20 (2.28 - 2.20)	46.12 - 1.53 (1.58 - 1.53)
No. unique observations	49,839	140,564
Completeness (%)	99.8 (99.9)	99.9 (99.4)
Multiplicity	7.1 (7.3)	7.3 (7.1)
Average I/σ(I) (%)	19.8 (2.1)	16.6 (2.77)
R-merge (%)[a]	0.066 (1.25)	0.077 (0.68)
R-meas[b]	0.072	0.083
CC1/2	0.999 (0.879)	0.999 (0.858)
Refinement statistics		
Resolution (Å)	37.02 - 2.20	46.12 - 1.53
No. of reflections work set	47,774	138,564
No. of reflections test set	1,998 (4%)	2,000 (1.4%)
R_{work}[b]	0.209	0.143
R_{free}[c]	0.246	0.194
No. protein atoms	2	2
No. water molecules	85	805
Overall B-factor (Å^2)	61.60	21.70
RMS deviations from ideal values		
Bonds (Å)	0.009	0.006
Angles (º)	1.10	0.98
Ramachadran plot		
Favoured (%)	97	98
Disallowed (%)	0.4	0

[a]$R_{merge} = \sum_{hkl}(\sum_i(|I_{hkl,I} - \langle I_{hkl} \rangle|))/\sum_{hkl,i} \langle I_{hkl} \rangle$, where $I_{hkl,i}$ is the intensity of an individual measurement of the reflection with Miller indices h, k, and l, and $\langle I_{hkl} \rangle$ is the mean intensity of that reflection. Calculated for $I > -3\sigma(I)$.

[b]Rmeas = ∑hkl{N(hkl)/[N(hkl)-1]}1/2 ∑i|Ii(hkl)- |/ ∑hkl∑iIi(hkl), where Ii(hkl) is the intensity of the ith measurement of an equivalent reflection with indices hkl.

[c]$R_{work} = \Sigma_{hkl}(||Fobs_{hkl}| - |Fcalc_{hkl}||)/|Fobs_{hkl}|$, where $|Fobs_{hkl}|$ and $|Fcalc_{hkl}|$ represent the observed and calculated structure factor amplitudes.

[d]R_{free} is equivalent to R_{work} but calculated using the reflections excluded from refinement in the test set.

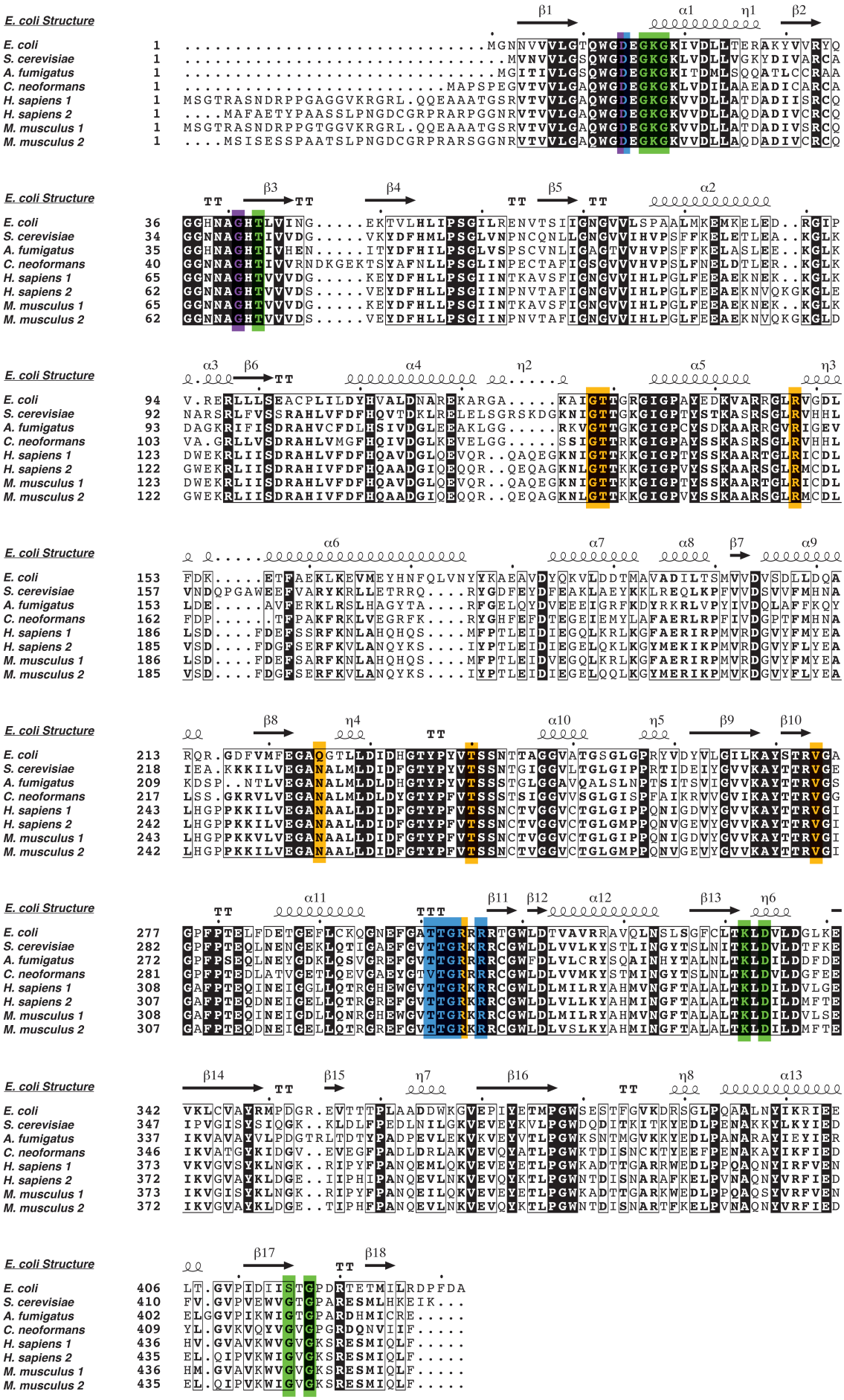
E. coli Structure
E. coli
S. cerevisiae
A. fumigatus
C. neoformans
H. sapiens 1
H. sapiens 2
M. musculus 1
M. musculus 2

Fig S1: Sequence alignment of AdSS genes from multiple species. Secondary structure elements from the *E. coli* structure annotated above. Colored columns indicate residues involved in substrate contacts, with orange indicating IMP-binding residues, green indicating GTP, blue indicating aspartate, and purple indicating magnesium.